Lund University GEM thesis series nr 18

Joint use of Sentinel-1 and Sentinel-2 for land cover classification: A machine learning approach

Miguel G. Castro Gómez

2017
Department of Physical Geography and Ecosystem Science
Lund University
Sölvegatan 12
S-223 62 Lund
Sweden

LUND UNIVERSITY

UNIVERSITY OF TWENTE.
FACULTY OF GEO-INFORMATION SCIENCE AND EARTH OBSERVATION

Joint use of Sentinel-1 and Sentinel-2 for land cover classification: A machine learning approach

by

Miguel G. Castro Gómez

Thesis submitted to the department of Physical Geography and Ecosystem Science, Lund University, in partial fulfilment of the requirements for the degree of Master of Science in Geo-information Science and Earth Observation for Environmental Modelling and Management

Thesis assessment Board

First Supervisor: *Hongxiao Jin* (Lund University)
Co-supervisors: Karlis Zalite (Tartu Observatory & Lund University)
Lars Eklundh (Lund University)

Exam committee:
David E. Tenenbaum
Enass Said Al-Kharusi

Disclaimer

This document describes work undertaken as part of a program of study at the University of Lund. All views and opinions expressed therein remain the sole responsibility of the author, and do not necessarily represent those of the institute.

Course title: Geo-information Science and Earth Observation for Environmental Modelling and Management (GEM)

Level: Master of Science (MSc)

Course duration: January 20*17* until June 20*17*

Consortium partners:

The GEM master program is a cooperation of departments at 5 different universities:
University of Twente, ITC (The Netherlands)
University of Lund (Sweden)
University of Southampton (UK)
University of Warsaw (Poland)
University of Iceland (Iceland)

ABSTRACT

Reliable information on land cover is required to assist and help in the decision-making process needed to face the environmental challenges society has to deal with due to climate change and other driving forces. Different methods can be used to gather this information but satellite earth observation techniques offer a suitable approach based on the coverage and type of data that are provided. Few years ago, the European Union (EU) started an ambitious program, Copernicus, that includes the launch of a new family of earth observation satellites known as Sentinel. Each Sentinel mission is based on a constellation of two satellites to fulfill specific requirements of coverage and revisit time. Among them are the Sentinel-1 and Sentinel-2 satellites. Sentinel-1 carries a Synthetic Aperture RADAR (SAR) that operates on the C-band. This platform offers SAR data day-and-night and in all-weather conditions. Sentinel-2 is a multispectral high-resolution imaging mission. The sensor has 13 spectral channels, incorporating four visible and near-infrared bands at 10 m resolution, six red-edge/shortwave-infrared bands at 20 m and three atmospheric correction bands at 60 m. The main objective of this study has been to investigate the classification accuracies of specific land covers obtained after a Random Forest classification of multi-temporal Sentinel data over an agricultural area. Four scenarios have been tested for the classification: i) Sentinel-1, ii) Sentinel-2, iii) Sentinel-2 and vegetation indices, iv) Sentinel-1, Sentinel-2, and vegetation indices. The classifications have been performed using a pixel and polygon based approach. The results have shown that the best accuracies (0.98) are obtained when using and polygon based approach independently of the scenario that is selected. For the pixel based approach, the highest accuracy (0.84) is obtained when using Sentinel-1, Sentinel-2, and vegetation indices.

Keywords: optical, SAR, land cover classification, Random Forest, temporal series.

ABSTRAKT

Tillförlitlig information om markskydd är nödvändig för att hjälpa och hjälpa till i beslutsprocessen som behövs för att möta de miljöutmaningar som samhället måste hantera tack vare klimatförändringar och andra drivkrafter. Olika metoder kan användas för att samla denna information, men satellitjordobservationstekniker erbjuder ett lämpligt tillvägagångssätt baserat på täckning och typ av data som tillhandahålls. För några år sedan inledde Europeiska unionen (EU) ett ambitiöst program, Copernicus, som inkluderar lanseringen av en ny familj av jordobservationssatelliter som kallas Sentinel. Varje Sentinel-uppdrag bygger på en konstellation av två satelliter för att uppfylla specifika krav för täckning och återkommande tid. Bland dem är Sentinel-1 och Sentinel-2 satelliterna. Sentinel-1 har en Synthetic Aperture RADAR (SAR) som fungerar på C-bandet. Denna plattform erbjuder SAR-data dag och natt och i alla väderleksförhållanden. Sentinel-2 är ett multispectral högupplösta uppdrag. Sensorn har 13 spektralkanaler, som innehåller fyra synliga och nära infraröda band med 10 m upplösning, sex red-edge / shortwave-infrarödband vid 20 m och tre atmosfärskorrigeringsband vid 60 m. Huvudsyftet med denna studie har varit att undersöka klassifikationsnoggrannheten för specifika markdäck som erhållits efter en slumpmässig skogs klassificering av flera temporala Sentinel-data. Fyra scenarier har testats för klassificeringen: i) Sentinel-1, ii) Sentinel-2, iii) Sentinel-2 och vegetationsindex, iv) Sentinel-1, Sentinel-2 och vegetationsindex. Klassificeringen har utförts med hjälp av ett pixel- och objektbaserat tillvägagångssätt. Resultaten har visat att de bästa precisionerna (0.98) erhålls vid användning och objektbaserad tillvägagångssätt oberoende av det scenario som väljs. För det pixelbaserade tillvägagångssättet erhålls högsta noggrannhet (0,84) när man använder Sentinel-1, Sentinel-2 och vegetationsindex.

Nyckelord: optisk, SAR, landskyddsklassificering, Random Forest, tidsserie.

ACKNOWLEDGMENTS

This research would not have been possible without the help and guidance of my supervisors. I would like to thank them for their work and support.

I would like to thank also professor Jonas Ardö for his help in the acquisition of the satellite imagery used for this research, and the team in charge of the SITES experiment.

I am grateful also to all the professors and staff involved in this Erasmus Mundus Master programme both at ITC Faculty – University of Twente and Lund University. Thank you for all your work.

Thank you to all my friends for their support and to Cecilia for keeping me on track and stay by my side.

Finally, my greatest thank to my family. Mamá, Papá, Amalia y Juan. Thank you for your support all this time. Nothing would have been possible without you.

TABLE OF CONTENTS

LIST OF FIGURES

LIST OF TABLES

LIST OF ABBREVIATIONS

BOA	Bottom Of the Atmosphere
CART	Classification And Regression Tree
CL Red-Edge	Chlorophyll Red-Edge
CM	Confusion Matrix
CRAN	Comprehensive R Archive Network
DOY	Day Of the Year
EPSG	European Petroleum Survey Group
ESA	European Space Agency
EU	European Union
EVI2	Two-band Enhanced Vegetation Index
EW	Extra Wide-swath
FAO	Food and Agriculture Organization
GDAL	Geospatial Data Abstraction Library
GLAM	Global Agricultural Monitoring Project
GMES	Global Monitoring for Environment and Security
GRD	Ground Range Detected
IRS-1A	Indian Remote Sensing Satellite 1A
IW	Interferometric Wide-swath
LAI	Leaf Area Index
NDVI	Normalized Difference Vegetation Index
NDWI	Normalized Difference Water Index
NIR	Near Infra-Red
OOB	Out Of the Bag
OSGeo	Open Source Geospatial Foundation
RADAR	Radio Detection And Ranging
RGB	Red-Green-Blue
S1	Sentinel-1
S2	Sentinel-2
SAB	Swedish Agricultural Board
SAR	Synthetic Aperture RADAR
SITES	Swedish Infrastructure for Ecosystem Science
SLC	Single Look Complex
SLU	Swedish University of Agricultural Science
SM	Strip Map
SNAP	Sentinel Application Platform
SPOT	Satellite Pour l'Observation de la Terre
TOA	Top Of the Atmosphere
USA	United State of America
UTM	Universal Transverse Mercator
VI	Vegetation Index
WGS	World Geodetic System
WV	Wave Mode

1. INTRODUCTION

1.1 Research background

Over the last decades, driving forces such as growing population, higher demand for supplies or energy needs are leading to a more extensive and intensive use of natural resources. Among others, the use of the available land is suffering the consequences of this shift in the global needs by forcing land use conversions and damaging the environment. One of the main changes is led by agricultural expansion and the necessity of increasing crop yields. The improvement of agricultural production can be achieved by using different techniques that vary greatly across the world (FAO, 2009) and, the expansion of arable lands is one of the options.

Following the necessity of better crop yields, the management of this resource has to be included in the discussion at different stakeholder levels. For example, farmers have to balance the use of irrigation systems, chemical fertilizers or pesticides with the environmental impact of these activities. By doing so, future scenarios where food production increases in the short-term but generates a long-term loss of ecosystem services, including those relevant for agriculture, can be solved (Foley, 2005). At a different scale, governments or international agencies require more detailed information that improves the decision-making process. Better crop-area identification, early estimation of production or validity of farmer's application for subsidies are just some examples where accurate and precise information is valuable.

One of the main tools used for the implementation of effective management decisions is agricultural mapping, which allows gathering information and statistics on crops and other related agricultural resources. Dealing with food security requires knowledge about the crop types and the land area that is being planted. In addition, data about the health and quality of the crops is essential to ensure the production levels. To collect the required data, one of the technologies that provides an economic and feasible approach for land cover information, and hence agricultural mapping, is remote sensing (Townshend, Justice, Li, Gurney, & McManus, 1991; Cihlar, 2000).

Remote sensing enables proper observation, identification, mapping, assessment, and monitoring of land dynamics at a range of spatial and temporal resolutions (Rogan & Chen, 2004). The increased availability of earth observation data together with the technological improvements in processing capacity are guiding the advance of remote sensing as a robust and consistent methodology (Gómez, White, & Wulder, 2016). As an example, the state of the land is highly dynamic so that the frequency of the necessary information about this system has to be coupled. Remote sensing provides the flexibility

to monitor agricultural areas, that switch from bare soil at the beginning of the season to high density vegetated areas at the peak growth.

The use of satellites for agriculture started in early 1970's (Bauer, 1973; Doraiswamy, Moulin, Cook, & Stern, 2003) when the first Landsat satellite (Landsat 1) was launched by the U.S.A. to classify Midwestern agricultural landscape into maize or soybean fields (Mulla, 2013). Then, new satellites were incorporated by other countries such as SPOT 1 (Satellite Pour l'Observation de la Terre – 1986, France) or IRS-1A (Indian Remote Sensing Satellite-1A – India, 1988), increasing the applications and possibilities of this technology. The large adoption of mapping and the inclusion of remote sensing as a relevant technology to address global applications has subsequently motivated the design of new and better satellite imaging systems. The main trends that lead the process are: resolution (spatial, temporal, radiometric and spectral), precision and information accuracy, processing data speed, and analysis capabilities (Wegener, 2001).

Remote sensing applications in agriculture are based on the interaction of electromagnetic radiation with vegetation or soil, by capturing the reflected radiation emitted by either an active or passive sensor. The electromagnetic region captured by a sensor determines the information that can be derived. Mainly, earth observation remote sensing focuses on the visible, infrared or microwaves regions and, based on that, two main classifications are done: optical and SAR (Synthetic Aperture RADAR) remote sensing.

Optical remote sensing uses the sun as an external source of irradiance and measures the reflected radiation from a surface in the visible and infrared part of the electromagnetic spectrum. In the visible part, green plants reflect radiation inversely related to the amount of radiation absorbed by their photosynthetic and accessory pigments. For example, the chlorophyll pigment absorbs most part of the radiation in the visible spectrum from 400 nm to 700 nm, especially at 430 nm (blue) and 660 nm (red) and leads to low reflectance in these bands. (Chappelle, Kim, & McMurtrey, 1992). Contrarily, plant reflectance is high in the near infrared (NIR) region (700-1300 nm) as result of leaf inter-cellular structure, canopy density, and canopy structure effects (Mulla, 2013). Using these plant reflectance characteristics, many studies have been developed for different purposes. Song et al., (2017) used medium resolution optical satellite imagery to estimate cultivation area for soybeans at a national scale. Becker-Reshef et al., (2010) developed a Global Agricultural Monitoring Project (GLAM) using remotely-sensed optical data and derived products for crop condition monitoring and production assessment. Prasad, Chai, Singh, & Kafatos, (2006) combined derived products from optical imagery with surface parameters to estimate crop yield. An extensive review optical remote sensing applications in agriculture was conducted by Wojtowicz, Wojtowics, & Piekarczyk,

(2015). Despite the progress made with optical sensors, it is not always possible to provide the desired information due to constraints related to cloud cover and revisit time.

The strong contrast of radiation absorption in the visible and infrared region of the spectrum makes possible to create quantitative indices of vegetation conditions. These mathematical quantitative combinations are known as vegetation indices. The usual form of a vegetation index is a ratio of reflectance measured in two bands or their algebraic combination. Some examples are NDVI (Rouse, Haas, Schell, & Deering, 1974), EVI2 (Jiang, Huete, Didan, & Miura, 2008), Cl-RedEdge, (Gitelson, Keydan, & Merzlyak, 2006; Gitelson, Gritz, & Merzlyak, 2003) and NDWI (Gao, 1996). Numerous papers have studied the use of vegetation indices for remote sensing applications either individually or in combination with spectral bands (Bannari, Morin, Bonn, & Huete, 1995; Mróz & Sobieraj, 2004; Dash et al., 2007; Campus et al., 2010)

Unlike optical, SAR satellites use their own source of radiation. The microwave electromagnetic radiation used depends on the applications of each mission, but they mainly operate at the X-band (2.5 – 3.75 cm), C-band (3.75 – 7.5 cm) or L-band (15 – 30 cm). By using active microwave radiation, SAR satellites can take advantage of its characteristics: penetration of waves in the ground (few centimetres), weather independence, and day-and-night imaging capability. Once the radiation is backscattered by a target, the sensor captures its strength and phase. The resulting value is directly linked with the wavelength, roughness, geometry, and material contents of the target.

When using SAR technology for imaging, the spatial resolution of the final image has to be considered. The final pixel size is defined by the azimuth resolution (direction parallel to the flight path) and the range resolution (direction perpendicular to the flight path). The azimuth resolution established that two objects on the ground, and with the same slant range (distance between antenna and target) can only be sensed separately if they are not both within the radar beam at the same time. For a specific frequency f (or wavelength λ), the azimuth resolution is entirely dependent on the aperture length of the antenna. So, high-resolution images in the azimuth direction require maximizing the diameter of antennas. However, space-engineering limitations make impossible to transport big devices. To solve this problem, the Doppler effect of echo signal can be used to synthesize artificially a much longer antenna aperture, and then produce images with higher spatial resolution. This type of procedure is used in all SAR satellites and that is the reason for its name: Synthetic Aperture RADAR. The range resolution is determined by the product of the speed of light by the pulse length divided by 2.

Many researches have explored the possibilities to use SAR in agriculture. Erten, Lopez-Sanchez, Yuzugullu, & Hajnsek, (2016) compared different techniques to use SAR data to retrieve vegetation height from space. Moran et al., (2012) analysed the applicability of SAR time series for monitoring crop and soil conditions. Hirooka, Homma, Maki, & Sekiguchi, (2015) used SAR data to evaluate leaf area index (LAI) in rice fields.

Due to the limitations in optical and SAR remote sensing technologies, there has been increasing interest in jointly using both of them for agricultural purposes, since combining both sensors can help in discriminating different classes (Pohl & Van Genderen, 1998). Many studies have performed multisensor analysis to improve mapping accuracy in agricultural scenarios (Ban, 2003; Brisco & Brown, 1995; Haack & Bechdol, 2000; Inglada, Vincent, Arias, & Marais-Sicre, 2016; Solberg, Jain, & Taxt, 1994).

1.2 About this study

Taking advantage of the efforts of the European Union (EU) to develop services based on satellite Earth Observation and in-situ data, this work aims at improving agricultural information based on a multisensor approach. A research is proposed to investigate the use of multi-temporal Sentinel-1 (SAR) and Sentinel-2 (Optical) satellite data, together with vegetation indices, for agricultural mapping.

The family of Sentinel satellites is included in the space component of the Copernicus program of the EU and the European Space Agency (ESA) (previously known as Global Monitoring for Environment and Security – GMES). The objective of this initiative is to improve the management of the environment, study climate change impact, and ensure civil security. Through satellites and in-situ observations (ground based weather stations, air quality monitoring networks, etc.) this service delivers near real time data on a global level for applications at different scales. The space segment is formed by 6 constellations of two satellites each, with a range of technologies from SAR to multi-spectral imaging.

The Sentinel-1 mission (formed by Sentinel-1A and Sentinel-1B satellites) is a polar orbiting day and night SAR imaging mission at an altitude of 700 km. Sentinel-1A was launched on April 3th 2014 and Sentinel-1B on April 25th 2016. The satellites work on the C-band, and in combination, their global revisit time is six days. There are four operation modes: interferometric wide-swath (IW) with a swath width of 250 km and 5x20 m^2 pixel resolution, wave-mode (WV) at 20x20 km^2 and 5x5 m^2 pixel resolution, strip map (SM) mode at 80 km swath width and 5x5 m^2 pixel resolution, and extra wide-swath (EW) at 400 km swath width and 20x40 m^2 pixel resolution. The satellite supports operations in a single (HH or VV) or dual polarization (VV+VH or HH+HV). Each Sentinel-1 product acquired in SM, IW and EW can be distributed at three processing levels: i) level-0

products are compressed and unfocused SAR raw data and are the basis from which higher level products are produced, ii) level-1 products are focused data and it is mainly designated for most data users. The processing from level-0 to level-1 includes Doppler centroid estimation, single look complex focusing, and image and post-processing for generation of the Single Look Complex (SLC) and Ground Range Detected (GRD) products. The SLC and GRD are two different level-1 sub-products, iii) level-2 consists of geolocated geophysical products derived from Level-1.

The Sentinel-2 mission (formed by Sentinel-2A and Sentinel-2B) is a polar orbiting multi-spectral imaging mission with 13 spectral bands at an altitude of 786 km. Sentinel-2A was launched on June 23th 2015 and Sentinel-2B on March 7th 2017. In combination, the two satellites provide a revisit time of 5 days at the equator. The 13 bands cover a range of the spectrum from 43 nm to 2190 nm with a swath width of 290 km and a spatial resolution of 10 m (4 visible and near-infrared bands), 20 m (6 red-edge/shortwave infrared bands), and 60 m (3 atmospheric correction bands). All data acquired by the satellite sensor is processed at different levels. The first one, Level-0, includes telemetry analysis, of low resolution image extraction and ancillary telemetry analysis among others. The second one, Level-1, is produced by using level-0 output and has three different sub-products: i) level-1A which decompresses relevant mission source packets, ii) level-1B which applies radiometric corrections to level-1A output, iii) level-1C where radiometric and geometric corrections (including orthorectification and spatial registration) are performed and Top Of the Atmosphere (TOA) are calculated. The third one, Level-2, includes a scene classification and an atmospheric correction applied to TOA values among others. The main output is then an orthoimage with Bottom Of the Atmosphere (BOA) reflectance values. It has to be highlighted that all the Sentinel-2 products are systematically processed to level-1C and that this is the unique level released for users from ESA. If desired, level 2A can be processed on the user side through specific software (Sentinel-2 Toolbox). Table 1 summarizes the Sentinel-2 characteristics.

Using remote sensing images for agricultural mapping requires the classification of the images into different crop types that are present in a specific area. Although many classification approaches have been developed, the selection of a specific algorithm is still one of the challenges when doing image classification. The selection requires the consideration of different factors such as computational resources, algorithm performance or classification accuracy (Defries & Chan, 2000). Algorithms can be per-pixel, subpixel, and per-field and the process can be either supervised or un-supervised.

In recent years, several algorithms developed for machine learning have been adopted for remote sensing applications. These include support vector machine, neural networks, and

Random Forest. In opposition to parametric classifiers, a machine learning approach does not start with a data model but instead learns the relationship between the training and the response dataset (Breiman, 2001). Over the last decades, the Random Forest algorithm has received increasing attention due to good classification results and the speed of processing (Du, Samat, Waske, Liu, & Li, 2015; Rodriguez-Galiano, Ghimire, Rogan, Chica-Olmo, & Rigol-Sanchez, 2012).

Table 1. Sentinel-2 specifications.

Band ID	Resolution (m)	Central wavelength (nm)	Band width (nm)
B01	60	443	20
B02	10	490	65
B03	10	560	35
B04	10	665	30
B05	20	705	15
B06	20	740	15
B07	20	783	20
B08	10	842	115
B08A	20	865	20
B09	60	945	20
B10	60	1375	30
B11	20	1610	90
B12	20	2190	180

The Random Forest classifier is an aggregated model, which means it uses the output from different models (trees) to calculate the response variable, in our case crop type. In recent years, a number of studies have reported that ensembles methodologies produce performance improvements over single base methods (Dahinden, 2009). Ensemble methods consist in learning several weak classifiers to generate a classifier with a strong decision rule. The combination of the tree's outputs can be achieved using weighted or unweighted voting to classify new samples. Bagging (Breiman, 1996) and Boosting (Freund & Schapire, 1996) are well-known representatives of this methodology.

To understand how Random Forest works, it is necessary to become familiar with decision trees. A known method to fit trees is CART (Classification And Regression Tree) (Breiman, Friedman, Olshen, & Stone, 1984). Decision trees are predictive models that recursively split a dataset into regions by using a set of binary rules to calculate a target value for classification or regression purposes. In our case, classification trees will be used. Trees are created in the following manner. Given a training set with *n* number of samples and *m* number of variables, a random subset of samples *n* is selected with replacement (bagging approach) and used to construct a tree. At each node of the tree, a

random selection of variables *m* is used and, out of these variables, only the one providing the best split will be used to create two sub-nodes. By using a subset and random selection of variables, less correlation among trees and lower error rates can be achieved.

The decision of which variable provides the best splitting criteria is made by using the GINI index (in CART algorithm). GINI index measures class homogeneity and as it increases, class heterogeneity increases as well. However, as GINI index decreases, class homogeneity increases. If a child node of GINI index is less than a parent node, then the split is successful. Tree splitting is finished when GINI index is zero. This means that only one class is present at each terminal node (Watts, Powell, & Lawrence, 2011).

To create the forest, the user can determine two parameters. The first one is the number of trees that will be created. Since Random Forest is computationally efficient and does not overfit, the number of trees can be as large as desired. However, previous studies have shown that 500 trees are enough because errors usually stabilize before this number is achieved (Lawrence, Wood, & Sheley, 2006). The second parameter that can be chosen is the number of variables that are randomly selected when creating a splitting point. If not selected, a default value can be used instead. The default value is calculated using the square root of the total number of variables (Gislason, Benediktsson, & Sveinsson, 2006). By growing the forest up to the number of trees the user has selected, the algorithm creates trees that have high variance and low bias (Breiman, 2001). Once the forest is created, about two thirds of the samples have been used to train the model (*in-bag* samples) and the remaining one third will be used for an internal cross validation technique (*out-of-the-bag* samples – OOB).

One of the features of a Random Forest classification is variable importance (VI). It indicates the influence of each variable on the classification. VI can be calculated in different ways but because the CART algorithm uses the GINI index, the VI is obtained using the Mean Decrease in GINI (MDG) and the Mean Decrease in Accuracy (MDA). At every split, one of the randomly selected variables is used and there is a resulting decrease in the GINI. The sum of all decreases in the forest due to a given variable, normalized by the number of trees forms produces the Mean Decrease in GINI (MDG). The MDA takes into account the difference between the OOB error resulting from a dataset obtained through random permutations of the values of the different variables and the OOB error resulting from the original data set (Breiman, 2001)

Once the forest is created, each pixel of a remote sensing image is classified by each tree, producing as many classifications as number of trees. Each tree votes for a class membership and then, the class with the maximum number of votes is selected as the final

class. Recently, many studies have shown the relevance of Random Forest for land cover mapping (Colditz, 2015; Stefanski, Mack, & Waske, 2013). A review of Random Forest applications in remote sensing can be founded in (Belgiu & Drăgu, 2016).

1.3 Thesis Structure

The thesis has been organized into six chapters. **Chapter 1**, Introduction, has presented a brief introduction to the problem, narrowing down the topic until the use of SAR and optical sensors in agriculture, and providing a description of Sentinel-1, Sentinel-2 and Random Forest. **Chapter 2**, Objectives, describes the main objective, secondary objectives, research questions, and hypothesis. **Chapter 3**, Methodology, explains the steps followed to carry out the research, from the selection of the datasets to the processing techniques and algorithms used for image analysis and classification. **Chapter 4**, Results, presents the output of all the steps followed. **Chapter 5**, Discussion, discusses the result and development of the methodology. Finally, **Chapter 6** presents the conclusions and recommendations.

2. OBJECTIVES

2.1 Main objective

To assess which classification approach and variable combination produce the best accuracy when using time series dataset of satellite remote sensing over an agricultural area.

2.2 Specific objectives

1- To determine the classification accuracy using Sentinel-1 data exclusively.
2- To determine the classification accuracy using Sentinel-2 data exclusively.
3- To determine if the combination of Sentinel-1 and Sentinel-2 data can improve the classification accuracy.
4- To investigate if the inclusion of vegetation indices improves the classification.
5- To analyse if the accuracy improves in a pixel based or in a polygon based classification approach.
6- To analyse the influence of multi-temporal data in classification accuracy both in a pixel and polygon based approach.

2.3 Research questions

1- Which level of accuracy can be obtained using Sentinel-2 data, taking into account its spatial and temporal resolution?
2- Can the combination of Sentinel-1 and Sentinel-2 increase the classification accuracy?
3- Do Sentinel-1 data add relevant information when classifying remote sensing data?
4- Do vegetation indices represent a valuable source of information when performing image classification?
5- Which classification approach is better for crop identification?
6- Could this combination of sensors improve crop management and decision making?
7- Can time series data add valuable information when mapping crop types?

2.4 Hypothesis

- A multisensor approach (Sentinel-1 and Sentinel-2) will produce better results in classification accuracy since both interact with the target in different ways, retrieving distinct and valuable information.
- Taking into account the spatial resolution of both satellites, the polygon based approach is expected to produce better results because it reduces mixed pixel and speckle effects of data.
- The use of time series will provide a temporal perspective of the growing season helping in the discrimination of the different classes.

3. METHODOLOGY

For this research, satellite imagery has been processed according to its characteristics to allow further image classification. Sentinel-1 images have been radiometrically corrected, terrain corrected, filtered for speckle noise, and cropped. Sentinel-2 images have been cropped as well and used to derived vegetation indices. After that, pixel based and polygon based Random Forest classifications were performed using different multi-temporal and multi-sensor datasets over an agricultural area. Finally, the accuracies were compared. Figure 1 shows a flowchart of the methodology used for the implementation of this research. Further details of each step can be found in the following sections.

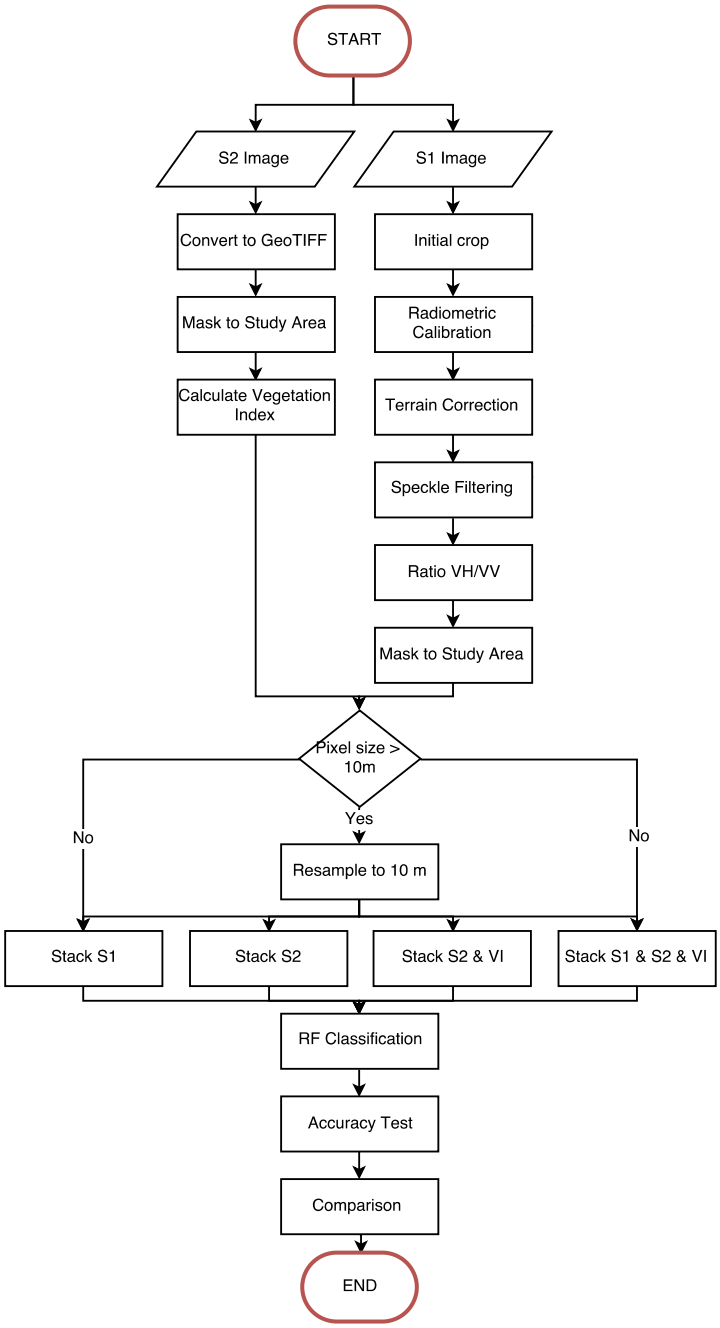

Figure 1. Flowchart of the methodology.

3.1 Study area

The site is located in Sweden, in the south of the Skåne region between the cities of Malmö and Lund (55.66 N, 13.16 W). The main land use in this region is agriculture which counts for 40 % of the total land cover. The region has an oceanic climate, with average temperatures during summer around 20 ºC and around 3 ºC during winter. The annual precipitation can reach values up to 650 mm. The study site covers an agricultural area primarily, where the major crops are wheat, barley, sugar beet and rape covering together the 59% of the study area. They represent the 22%, 14%, 12%, and 11% of the agricultural fields respectively. In addition, some built-up zones and other minority crops can be found as well. The total coverage is about 67 km^2, with approximately 10 km in the west-east direction and 6 km in the north-south. For this study, only the main land covers will be taken into account for the classification. Those are winter wheat, barley, rapeseed, sugar beet and built-up areas. The remaining classes will be considered as "others". Figure 2 shows the location of the study area. Figure 3 shows the extent of the selected land covers compared to the total extension of the study area.

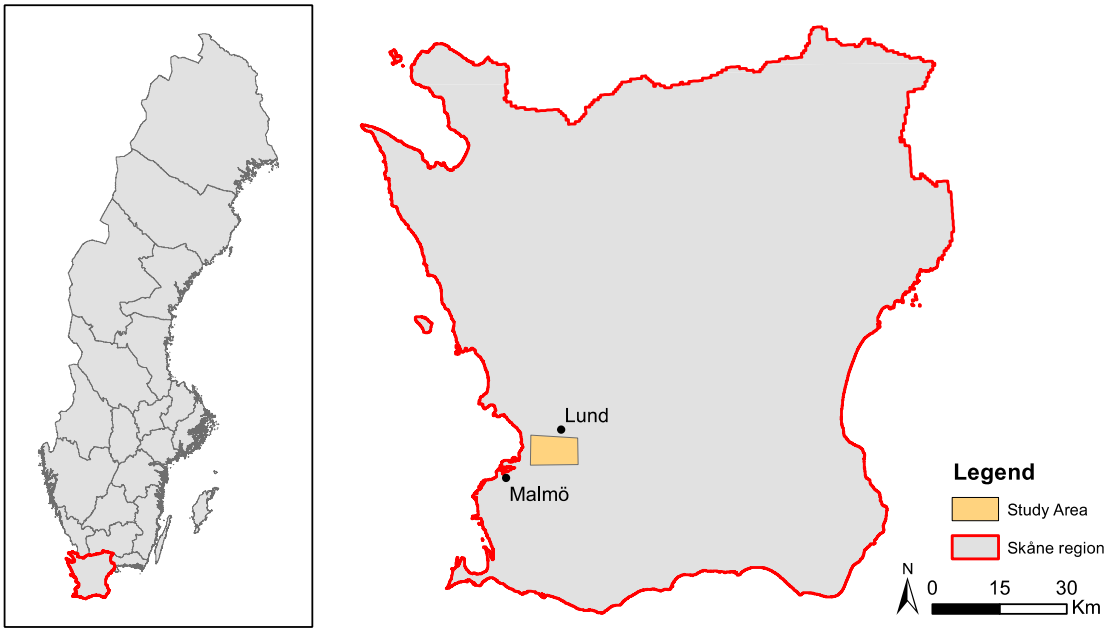

Figure 2. Study area. The left figure shows the location of the Skåne region inside Sweden. The right figure shows the location of the study area (orange) inside the Skåne region.

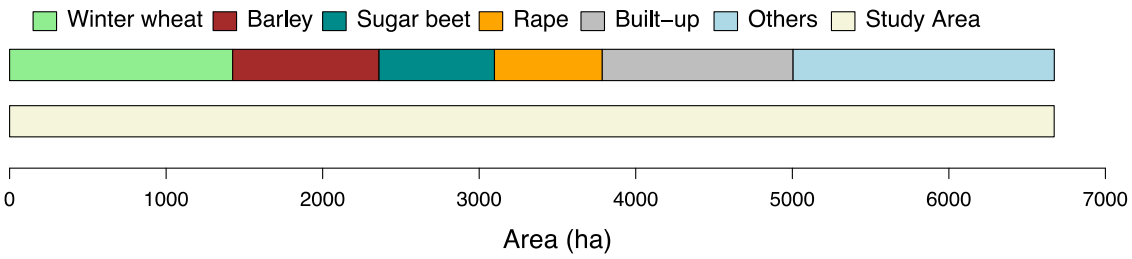

Figure 3. Area (in ha) of land covers inside the study area. The lower bar shows the total extension of the study area. The higher bar shows the area of each land cover.

3.2 Projection

All the satellite imagery, as well as additional datasets, are referenced in a projected coordinate system. The geographic coordinate system used is the World Geodetic System 84 (WGS 84) and the selected projection is Universal Transverse Mercator zone 33N (UTM zone 33N). The identifier of the projection is EPSG 32633.

3.3 Sentinel-2

3.3.1 Data

Using as reference the tiling grid system of Sentinel-2 products, all the cloud-free images and those with a low percentage (visually determined) of cloud cover available during the growing season for the tile 33UUB were considered as inputs for this study. In total, a dataset of 12 images was used. Images were downloaded from the Copernicus Open Access Hub of the European Space Agency (ESA) as Level-1C which means that those products are ortho-images in UTM/WGS84 projection, with per-pixel radiometric measurements provided in Top Of the Atmosphere (TOA) reflectance. The decision of choosing level 1C as the level for the optical imagery used in this project is based on the final objective of this study. Classification purposes do not always require the correction of atmospheric effects (C. Song, Woodcock, Seto, Lenney, & Macomber, 2001) especially if the spectral signatures characterizing the desired classes are derived from the images to be classified (Fraser, Bahethi, & Al-Abbas, 1977; Potter, 1974). Atmospheric correction would not be expected to increase classification accuracy but only to attain an estimation of the reflectance at the bottom of the atmosphere. Table 2 shows the dates of the Sentinel-2 images.

Table 2. Sentinel-2 image acquisition dates

DATE	Δ Days	DOY (2016)
2016-04-22	-	113
2016-05-02	10	123
2016-05-05	3	126
2016-05-12	7	133
2016-05-22	10	143
2016-05-25	3	146
2016-06-04	10	156
2016-06-24	20	176
2016-07-11	17	193
2016-07-21	10	203
2016-07-24	3	206
2016-07-31	7	213

3.3.2 GDAL pre-processing

Once downloaded, all the bands of the 12 images were converted from its original format (jpeg2000) to GeoTIFF. The procedure was done using the Geospatial Data Abstraction

Library (GDAL) translator library, licensed by the Open Source Geospatial Foundation (OSGeo) version 2.1.2, released on 2016/10/24.

3.3.3 R processing

After the format conversion, images were processed to homogenize the different spatial resolutions (10 meters bands 2, 3, 4, 8 – 20 meters bands 5, 6, 7, 8a, 11, 12 – 60 meters bands 1, 9, 10). This step is required to make them ready for the Random Forest classification. The process was performed using the R software and the rgdal and raster packages. The final spatial resolution chosen for all the bands is 10 m since this is the highest resolution that can be found in a Sentinel-2 product and the one that captures the highest level of details. By downscaling images from 20 or 60 meters pixel resolution to 10 meters resolution, any original reflectance value is not lost and the original data are not changed except for the total number of pixels the images have. The opposite procedure, to upscale images from 10 meters to 20 or 60 meters, would have caused the loss of reflectance detail and a homogenization of the 10 meters bands and the advantage of the high resolution Sentinel-2 data would not be fully explored. Additionally, this smoothing process would affect bands in the visible and NIR part of the electromagnetic spectrum, which have useful information concerning vegetation.

The procedure starts by cropping the band images to the size of the study area. This steps also helps to decrease the computation time of the following steps. Each cropped band image is then resampled depending on its original spatial resolution. The resampling is done by creating a new raster that is fitted on top of the cropped band image and with the same extension. The pixel size of the new raster is set to 10 m. The resampling method used to transfer pixel values is the nearest neighbour method. This method ensures that each pixel value is transferred correctly to its corresponding new pixel. Figure 4 shows a representation of the method for a 20x20 m^2 raster. Figure 5 shows the same process for a 60x60 m^2 raster. For visualization purposes, the raster figures are not overlaing.

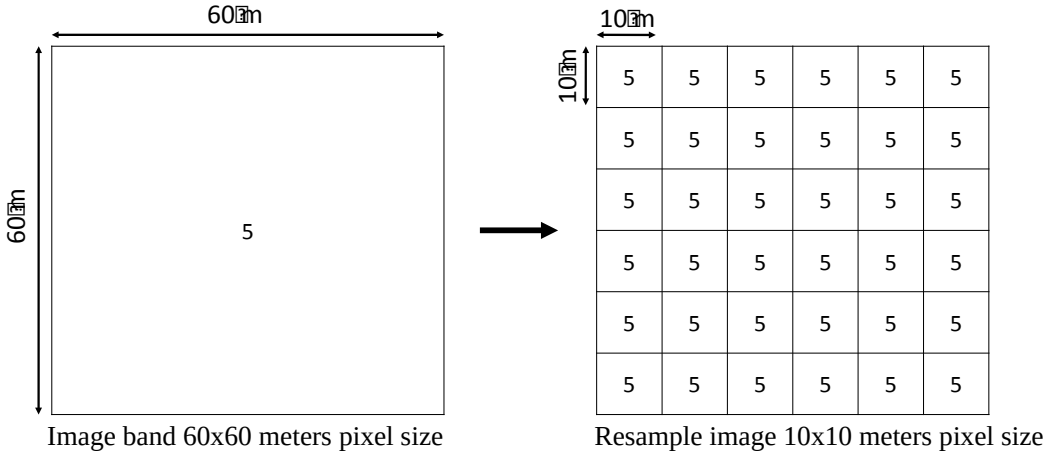

Figure 4. Resampling methodology for a 20x20 meters raster. The left figure shows the original raster. The right figure shows the output produced by the nearest neighbour method.

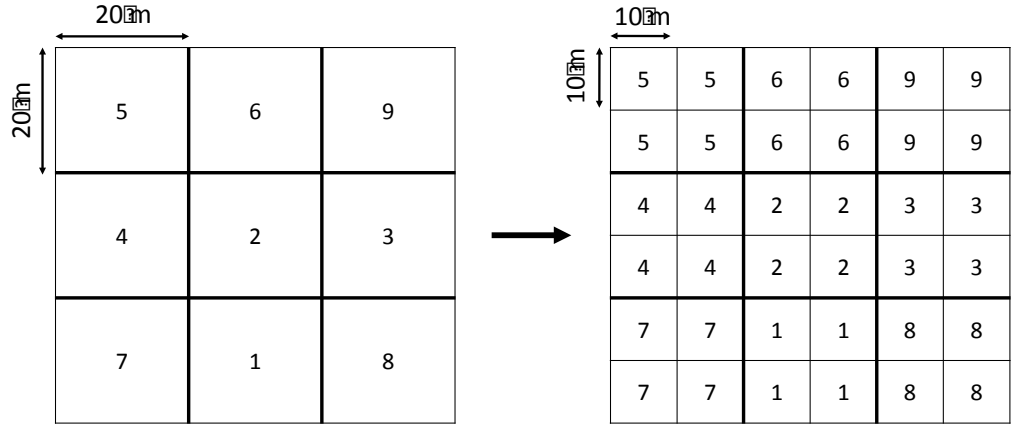

Image band 20x20 meters pixel size Resample image 10x10 meters pixel size

Figure 5. Resampling methodology for a 60x60 meters raster. The left figure shows the original raster. The right figure shows the output produced by the nearest neighbour method.

3.4 Vegetation indices

A selection of 4 of the main vegetation indices used for remote sensing of agriculture has been chosen for this study. Their use is justified since they add valuable information that can help to distinguish different land cover classes. In some cases, vegetation indices can add more class separability than the data acquired by individual spectral wavebands. For each available image, the following vegetation indices have been derived: Normalized Difference Vegetation Index (NDVI), Two-band Enhanced Vegetation Index (EVI2), Normalized Difference Water Index (NDWI), Chlorophyll Red-Edge ($Cl_{Red\text{-}edge}$). Table 3 presents the corresponding formulas used in each case.

Table 3. Formulas of the vegetation indices used in this research.

Index	Formulation S-2	Reference
$Cl_{Red\text{-}edge}$	$\left(\frac{Band\ 7}{Band\ 5}\right)$-1	(Gitelson et al., 2003, 2006)
NDVI	$\left(\frac{Band\ 8 - Band\ 4}{Band\ 8 + Band\ 4}\right)$	(Rouse et al., 1974)
NDWI	$\left(\frac{Band\ 8 - Band\ 11}{Band\ 8 + Band\ 11}\right)$	(Gao, 1996)
EVI2	$2.5 * \left(\frac{Band\ 8 - Band\ 4}{Band\ 8 + 2.4 * Band\ 4 + 1}\right)$	(Jiang et al., 2008)

3.5 Sentinel-1

3.5.1 Data

In order to combine Sentinel-2 images with Sentinel-1 images, a dataset has been selected so that each Sentinel-2 image has a corresponding Sentinel-1 image with the same sensing date. When this was not possible, a margin of ±7 days from the sensing date of a Sentinel-2 image was used to select the corresponding Sentinel-1 image. The margin of days has been decided based on the dynamics of the target area, which usually does not change on

a weekly basis (except for the harvesting period). As with Sentinel-2, Sentinel-1 images were downloaded from the Copernicus Open Access Hub of the ESA. In total, a dataset of 10 images have been selected with the following characteristics: dual polarization VV+VH mode, Interferometric Wide (IW) sensing mode and Ground Range Detected (GRD) product type. When possible, an ascending orbit was preferred to a descending one. Table 4 shows the dates of the Sentinel-1 images.

Table 4. Sentinel-1 image acquisition dates

DATE	ΔDays	DOY (2016)	Orbit
2016-04-26	-	117	Ascending
2016-05-08	12	129	Ascending
2016-05-20	12	141	Ascending
2016-06-01	12	153	Ascending
2016-06-06	5	158	Ascending
2016-06-30	24	182	Ascending
2016-07-12	12	194	Ascending
2016-07-19	7	201	Ascending
2016-07-24	5	206	Ascending
2016-07-31	7	213	Ascending

The dual polarization VV+VH was selected since the vertically-polarised electromagnetic field of the SAR interacts more strongly with the vertical stalks of a field of grains than would, say, a horizontally-polarised radar. Such interaction leads to differences in the power scattered back in those different polarizations. In addition, the specific structure of vegetation can cause a change in the orientation of the electromagnetic field from vertical to horizontal. Due to this, the VH polarization was also added. The dual VV-VH polarizations were selected in line with the results of previous studies that found these polarizations useful in crop classification (De Wit & Clevers, 2004; McNairn, Champagne, Shang, Holmstrom, & Reichert, 2009)

The Interferometric Wide (IW) mode was chosen since it is the main and default operational mode over land of the Sentinel-1 satellite. The remaining ones (Stripmap – SM; Extra-Wide swath – EW; Wave - WV) where not taken into account because either they are primarily used for wide area coastal monitoring (EW), only available upon request for extraordinary events (SM), or do not have a dual polarization (WV).

The Ground Range Detected (GRD) product type was used because they have been the multi-looked and projected to ground range. Although phase information of the signal is lost, for classification purposes the backscatter information is enough. In addition, pixels have approximately square resolution (20x22) and square pixel spacing (10x10 meters) which makes it easier to combine with Sentinel-2 data.

The preference for an ascending orbit is based on the timing of the acquisition in the case of Sentinel-1. Ascending orbit senses usually at 16:50 p.m. approx. over the study area while a descending orbit would sense around 05:30 a.m. approx. Choosing the latest time of sensing allows preventing the absorption of the microwave radiation by water that could have been condensate during the night on the fields.

3.5.2 Pre-processing

Once the images were downloaded, a pre-processing chain was required to correct the SAR products. SAR images have to be radiometrically corrected, terrain corrected, and filtered due to speckle noise. In addition, an extra step has been added to this pre-processing chain to calculate a ratio between the backscattered radiation of the VH and VV bands. The complete process is done using the intensity bands of the Sentinel-1 products. The software used for this process is the Sentinel Application Platform (SNAP), provided free of charge by the ESA.

Crop

By decreasing the extension of the original product to one slightly bigger than the study area, the size of the input is reduced considerably. This helps to speed up the remaining steps and reduce the number of computational operations. The latitude/longitude coordinates of the polygon used to reduce the size of the original products are: i) 55º19'33'' – 012º 51'49''; ii) 55º19'33'' – 013 º40'33''; iii) 55º52'04'' – 013 º40'33''; iv) 55º52'04'' – 012º 51'49''.

Radiometric calibration

Once cropped, the pixel values of the images have to be transformed so that they represent a measurement of the ground reflectivity or radar cross-section. The power of the received radar signal also accounts for factor such as antenna gain, system loss, etc. This introduces a significant radiometric bias in the SAR image. The radiometric calibration is done by calculating the sigma nought (σ^0) or normalized radar cross-section coefficient. The produced output is a normalised measure of the radar return from a distributed target.

Terrain correction

Because of the side looking geometry of a SAR system, every target located on the terrain being observed by the radar will be mapped onto the slant range domain. The terrain correction is the process by which SAR data are converted from slant range to ground range geometry and in a defined cartographic system. SAR images are likely to be affected by geometric distortions and the most commons are: i) foreshortening (occurs when the radar beam reaches the base of a tall feature tillted towards the radar before it

reaches the top. The slope will appear compressed and the length of the slope will be represented incorrectly at the image plane), ii) layover (occurs when the radar beam reaches the top of a tall feature before it reaches the base. The return signal from the top of the feature will be received before the signal from the bottom. As a result, the top of the feature is displaced towards the radar from its true position on the ground, and, lays over the base of the feature (b' to a') iii) shadow (increases with greater incident angle θ, just as our shadows lengthen as the sun sets). The terrain correction process is done using the Range Doppler Terrain Correction tool of SNAP, which automatically downloads and uses the Digital Elevation Model provided by the NASA Shuttle Radar Topography Mission with a resolution of 3 arc-seconds. The resampling procedure is the bilinear interpolation method. The output of the terrain correction step is a geocoded image.

Speckle filtering

Speckle noise-like feature is a common phenomenon in SAR systems. It confers to SAR images a granular aspect and random spatial variation. The source of this noise is attributed to random interference between the coherent returns. The principle of speckle filtering is to reduce the variance of the complex speckled scattering and improve the estimate of the unspeckled scattering coefficient. The Lee sigma filter has been used for this research. The selection is based on previous studies that demonstrate that the Lee Sigma algorithm performs better than other speckle filters (Lee, Wen, Ainsworth, Chen, & Chen, 2009; Meenakshi & Punitham, 2011). The parameter values were set to the default values provided by SNAP when selecting this filter. Table 5 shows the parameters of the speckle filter used.

Table 5. SAR Speckle filtering parameters.

Parameter	Value
Filter	Lee sigma
Number of looks	1
Window size	7x7
Sigma	0.9
Target window size	3x3

Ratio calculation

A new product consisting of the ratio between the pixel values of the intensity band in VH and VV has been calculated for each image. This allows deriving relevant information that can help to differentiate classes. The result is obtained using the raster calculator included in the SNAP software.

3.5.3 R processing

After the pre-processing steps performed in SNAP, SAR images require extra processing to make them ready for the Random Forest classification. Images have to be cropped to the size of the study area. The process is similar to the one performed for Sentinel-2 images but, since Sentinel-1 GRD products have already 10x10 m^2 pixel spacing, this characteristic does not need to be modified.

3.6 Sentinel-1 & Sentinel-2 data

By combining the two sensor datasets, a total of 22 images were made available for this project. Table 6 shows the dates of Sentinel-2 images and the corresponding Sentinel-1 image between a range of ±7 days. Due to the lack of Sentinel-1 images over the study area for some specific dates, the Sentinel-2 images of 2016-05-02 and 2016-05-05 uses the same Sentinel-1 image of 2016-05-08. The same situation happens for 2016-05-12 and 2016-05-22, which have both the Sentinel-1 image of 2016-05-20 as a reference. Due to this, there are 12 Sentinel-2 images and 10 Sentinel-1 images. Figure 6 shows the temporal distribution of the images as Days of Year (DOY).

Table 6. Combination of Sentinel-1 and Sentinel-2 image acquisition dates

Date	±Δ Days	Satellite
2016-04-22	4	Sentinel-2
2016-04-26		Sentinel-1
2016-05-02	6	Sentinel-2
2016-05-08		Sentinel-1
2016-05-05	3	Sentinel-2
2016-05-08		Sentinel-1
2016-05-12	8	Sentinel-2
2016-05-20		Sentinel-1
2016-05-22	-2	Sentinel-2
2016-05-20		Sentinel-1
2016-05-25	7	Sentinel-2
2016-06-01		Sentinel-1
2016-06-04	2	Sentinel-2
2016-06-06		Sentinel-1
2016-06-24	6	Sentinel-2
2016-06-30		Sentinel-1
2016-07-11	1	Sentinel-2
2016-07-12		Sentinel-1
2016-07-21	-2	Sentinel-2
2016-07-19		Sentinel-1
2016-07-24	0	Sentinel-2
2016-07-24		Sentinel-1
2016-07-31	0	Sentinel-2
2016-07-31		Sentinel-1

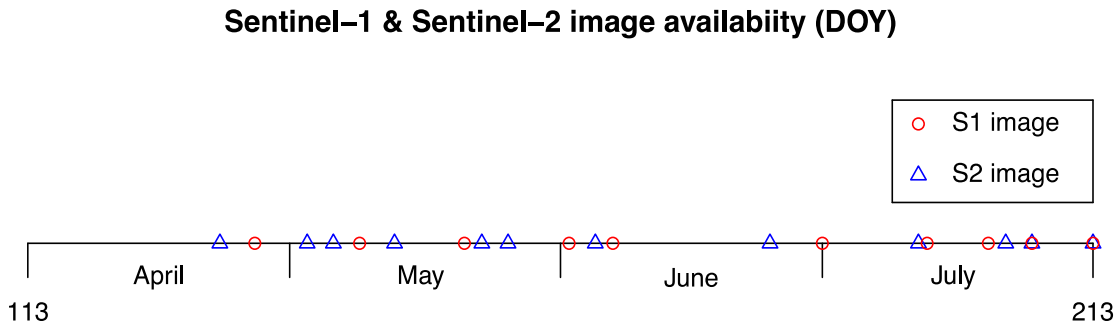

Figure 6. Temporal distribution of Sentinel-1 and Sentinel-2 images over the year 2016.

3.7 Growing season

The selection of the satellite imagery was coordinated with the growing calendar of the different crops of interest. This information has been provided by the Swedish University of Agricultural Sciences (SLU) researchers that manage the SITES experimental fields located inside the study area. This time perspective can improve the class differentiation and the quality of the classification. In addition, using the growing calendar helps to be sure that our fields were not being used for any other purpose than cultivating the crops we wanted to identify. For this reason, the latest sowing period and the first harvesting period were used as a reference. Using images (if available) from November 2015 or February 2016 would have added uncertainty to the final classification. Figure 7 shows the growing season of the crop types included in this study together with the available satellite imagery. Sowing and harvesting periods do not show specific dates since this can vary based on the decisions of farmers or specific field conditions. Harvesting periods start when the maximum growth is reached.

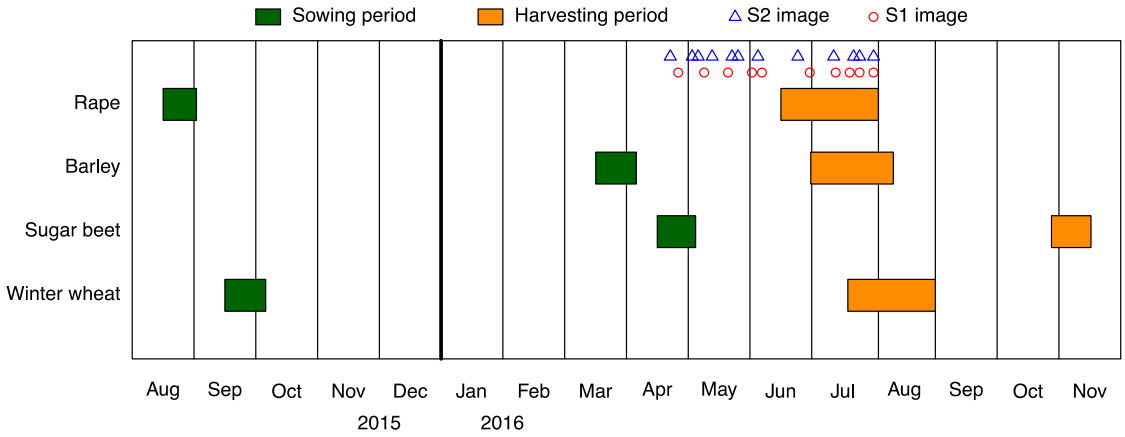

Figure 7. Growing season of the crop types selected for this study. The dates of the satellite imagery datasets are shown as well.

3.8 Classification scenarios

Two different approaches have been selected to classify the images: pixel-based and polygon-based. The first approach performs the classification using the information at the pixel level in opposition to the polygon based approach which uses information at the field/polygon level. The boundaries of those polygons are provided by the SAB dataset.

For each polygon, the mean value of pixels inside is calculated. Each approach consists of 4 different scenarios where the input data presented previously varies. Using both a pixel and polygon based classification helps to maximize the information that could be extracted from the sensors. Although optical remote sensing produces relevant information at the pixel level, SAR data can be less effective at this level for some applications such as agricultural mapping. The characteristics of this product create difficulties to have homogeneous reflectance values over an area with similar characteristic. SAR images are known for suffering the *salt-and-pepper* effect, where one pixel can have a very high value and the one to the left a very low value. Since the main purpose of this research was to classify agricultural fields, the polygon based approach was suitable to deal whit this feature. Table 7 summarises the classification scenarios.

Table 7. Classification scenarios used for this research

Input Pixel-based	Input Polygon-based
Sentinel-1	Sentinel-1
Sentinel-2	Sentinel-2
S2 & vegetation indices	S2 & vegetation indices
S1 & S2 & vegetation indices	S1 & S2 & vegetation indices

To assess the influence of multi-temporal data in accuracy levels, the classification scenarios described previously are run using a progressive number of inputs starting only with one image and ending with the complete dataset of each scenario.

3.9 SAB data

Figure 8 presents the dataset of the year 2016 of the Swedish Agricultural Board (SAB) that has been used as reference data for this study. It consists of polygons representing the cadastral limits of the fields in the study area. Each polygon contains information such as the region of the country where the polygon is, the area, or the crop type that is been cultivated this year. For this study, only the boundaries and the crop type information have been used. The statistical information is collected by this organization with the help of farmers, which have to inform about the crop type they are planting on their fields. The decision of the land cover that will be classified was made from this dataset.

3.10 Training dataset

To perform the supervised classification proposed in this research, a training set is required. It allows the algorithm to learn the relation between the pixel values of the different image bands and the land cover class. For this purpose, a training set has been designed for this project using a stratified random sampling approach. For each one of the six land cover classes, 50 points have been selected randomly.

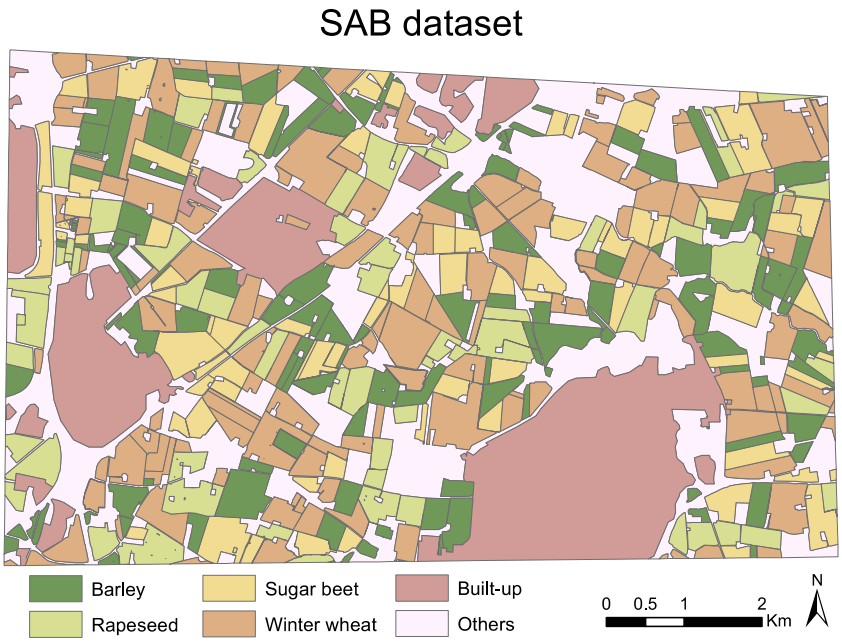

Figure 8. Swedish Agricultural Board (SAB) reference data.

3.11 Random Forest Classification

Following the scenarios described in the previous section, a Random Forest classification is run for each one. For the process, the Random Forest package version 4.6-12 of the Comprehensive R Archive Network (CRAN) implemented by Liaw and Wiener (Liaw & Wiener, 2002) was used. The process starts by stacking the SAB data layer to the set of images that will be used in each classification scenario. After that, the 300 training points (50 per class) are used. At their location, the values of each layer are extracted and saved in a table where each row represents a point and each column an image band. During the following step, the Random Forest classification model is trained using the training set. At this moment, the trees of the forest are created using the image bands to make split decisions. For this study, 500 trees have been created and the number of variables used correspond to the square root of the total amount of inputs in each scenario. Finally, after the training, the resulting Random Forest model is used to classify the inputs of each scenario and to extract the corresponding variable importance measures.

3.12 Accuracy evaluation

Once the classification is finished, it is necessary to know the accuracy of the process. For this purpose, a validation dataset is created. It consists, as the training dataset, of 50 (different) random points selected for each class (300 points in total). The accuracy evaluation performs a cross-validation at those point locations comparing the class value from the SAB reference data versus the class obtained by the classification algorithm. This comparison produces an accuracy percentage and the kappa statistic.

4. RESULTS

The present chapter introduces the results of all the steps that were taken to develop this research, from the pre-processing and processing of Sentinel-1 and Sentinel-2 images to the calculation of vegetation indices. The classifications obtained according to the different settings explained in the previous chapter are also shown. Due to the processing chain, each input image produces a high number of outputs. For this reason, the Sentinel-2 image from May 25th, 2016 has been used as an example to show the intermediate results. For Sentinel-1, the corresponding image from June 1st, 2016 has been chosen.

4.1 Sentinel-2

4.1.1 Sentinel-2 original data

Figure 9 shows an RGB composite (bands 4-3-2 for red, green, and blue bands, resolution 10m) of an original Sentienl-2 level 1C product. It can be observed a low coverage of clouds over the complete area and the study area.

4.1.2 Sentinel-2 R results

Figure 9. Original Sentinel-2 product. The image is shown as an RGB composite. The study area is represented by the red rectangle.

Figure 10 shows the same image, in an RGB (4-3-2) composite after it has been processed in R and cropped to the size of the study area. The difference in the colour intensity is due to the colour stretching process. Since the image size is reduced, the minimum and maximum values have changed and the distribution of colours is affected. This affects only to the visualization and not to the real data of the pixels.

Figure 10. RGB composition of a Sentinel-2 image cropped to the size of the study area.

Figure 11 shows the band 6 (20 meters spatial resolution) of the same Sentinel-2 product, with a panchromatic colour scale after it has been resampled to 10 meters resolution.

Figure 11. Band 6 of a Sentinel-2 image. A grey scale is used to represent reflectance values.

Since the resampling process does not produce any visual change, the histograms of the band 6 before and after the process are shown in Figure 12. It can be observed that the frequency of the pixel values is exactly 4 times the original one. The same result is obtained when processing the remaining bands of the product.

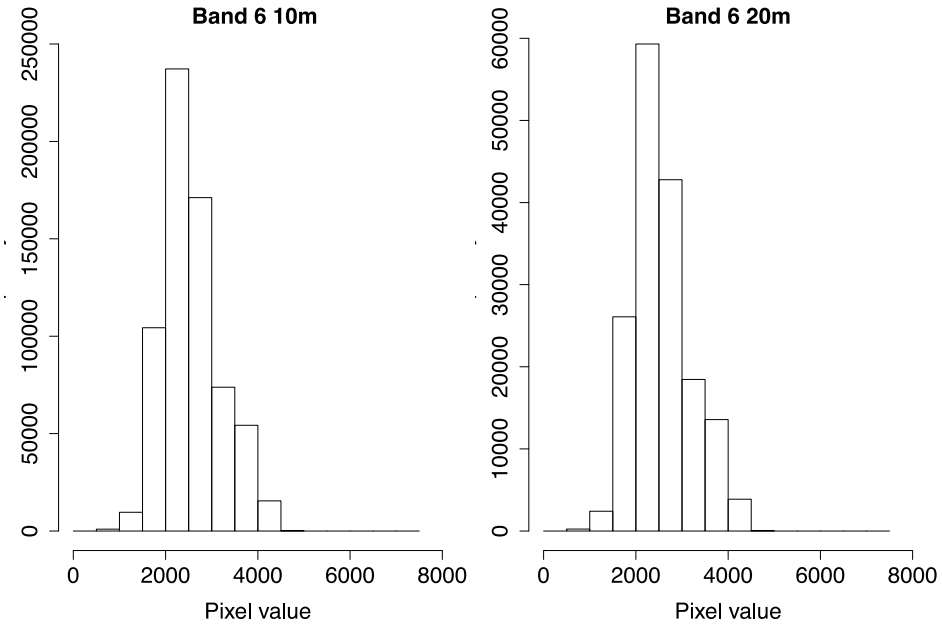

Figure 12. Histograms band 6 before (left) and after (right) resampling

4.2 Vegetation indices

The following figures show the 4 vegetation indices calculated for the Sentinel-2 product used as an example. Figure 13 shows the Normalized Difference Vegetation Index (NDVI), Figure 14 shows the Normalized Difference Water Index (NDWI), Figure 15 shows the Two-band Enhanced Vegetation Index (EVI2) and Figure 16 shows the Chlorophyll Red-Edge ($Cl_{Red\text{-}edge}$) index. A colour scale has been used to represent index values. Green represents high values for each index while red is used for low values. Differences within the agricultural area can be observed.

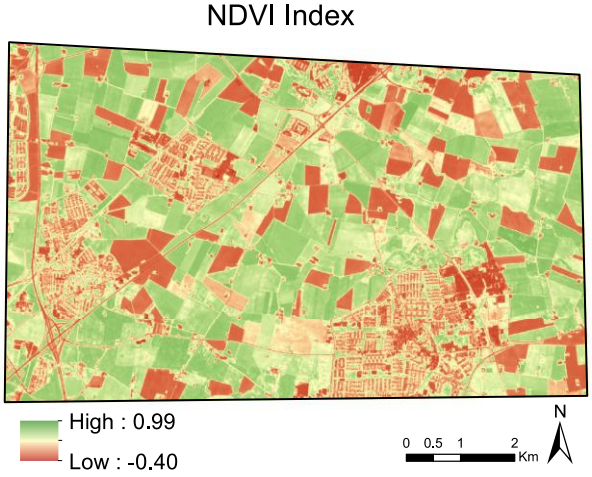

Figure 13. NDVI Index

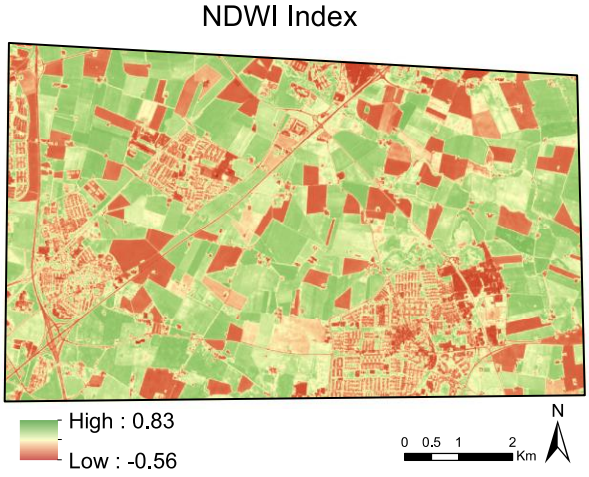

Figure 14. NDWI Index

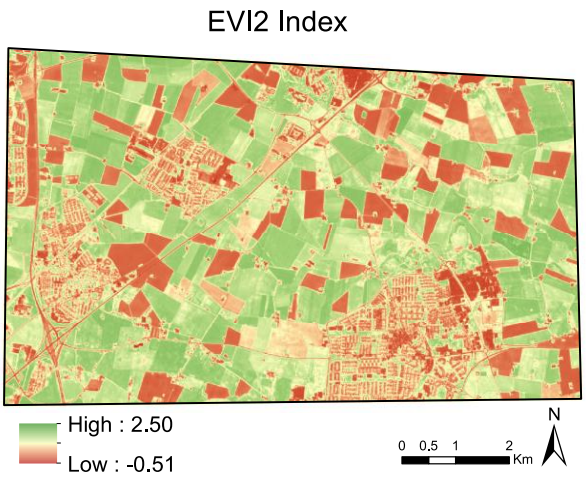

Figure 15. EVI2 Index

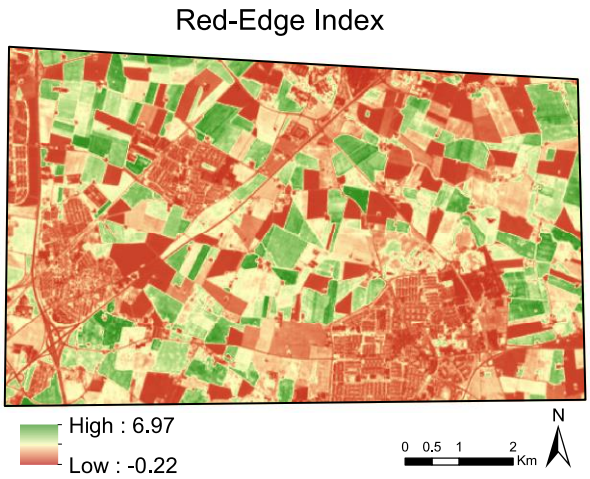

Figure 16. Red-Edge Index

4.3 Sentinel-1

4.3.1 Sentinel-1 original data

As mentioned previously, the Sentinel-1 product from June 1st, 2016 has been selected as an example to show the results produced during the processing of the SAR images. Figure 17 shows the intensity band in VV and VH polarization mode before any processing is done. Due to the acquisition geometry (ascending orbit) the image is flipped. The yellow arrow indicates the north direction. The blue arrows indicate the sensing direction. The study area is represented by the orange rectangle.

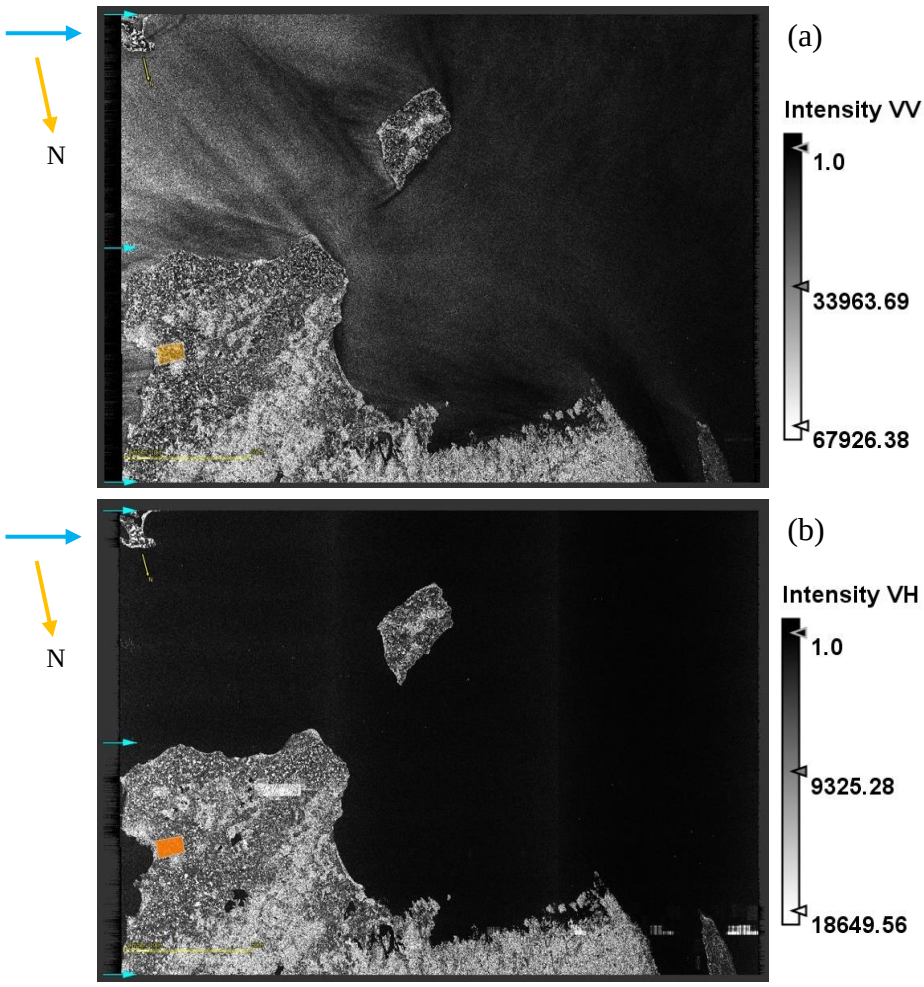

Figure 17. Original S1intensity band in VV (a) and VH (b) polarization mode.

4.3.2 Sentinel-1 SNAP processing

Figure 18 shows the result of the cropping process for the VV (a) and VH (b) intensity band. As we can see, the extent and size of the images have changed remarkably, allowing better computing performances in further steps.

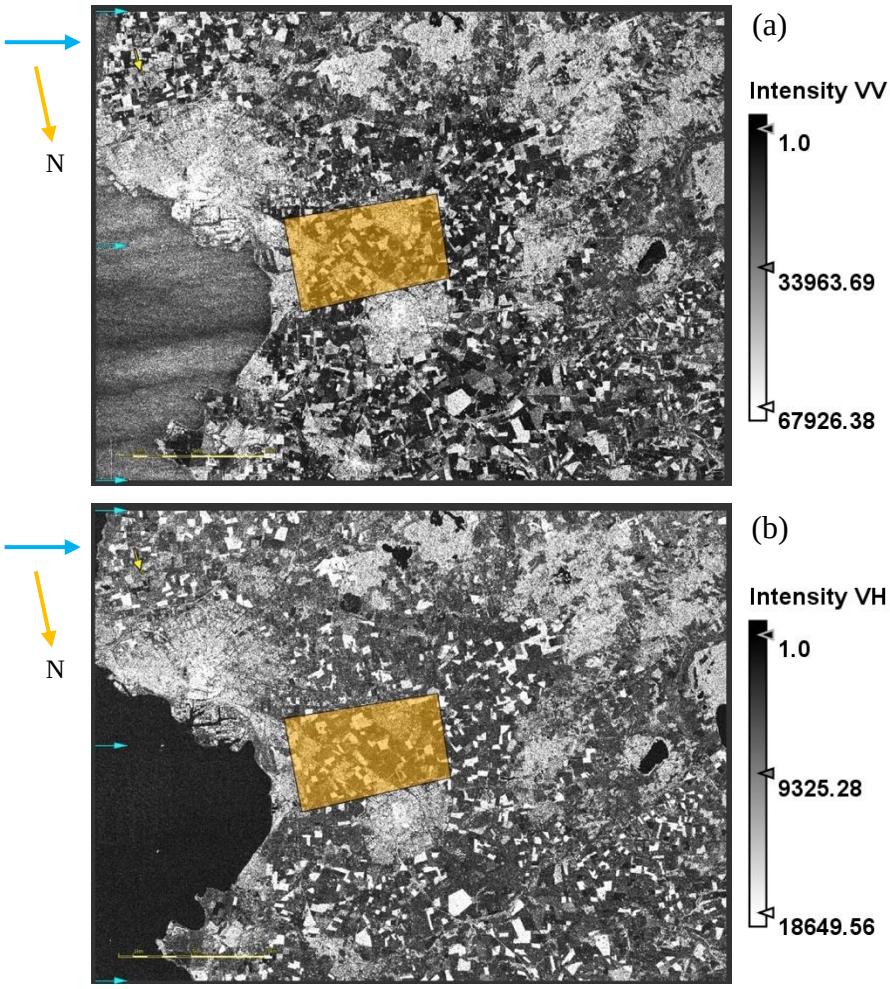

Figure 18. Cropped Sentinel-1 intensity band in VV (a) and VH (b) mode.

Figure 19 shows the results of the radiometric calibration process for the VV (a) and VH (b) intensity band. It can be observed that the brightness and intensity of the colour have changed due to this calibration process that allows to better represent the characteristics of the interaction between targets and radiation.

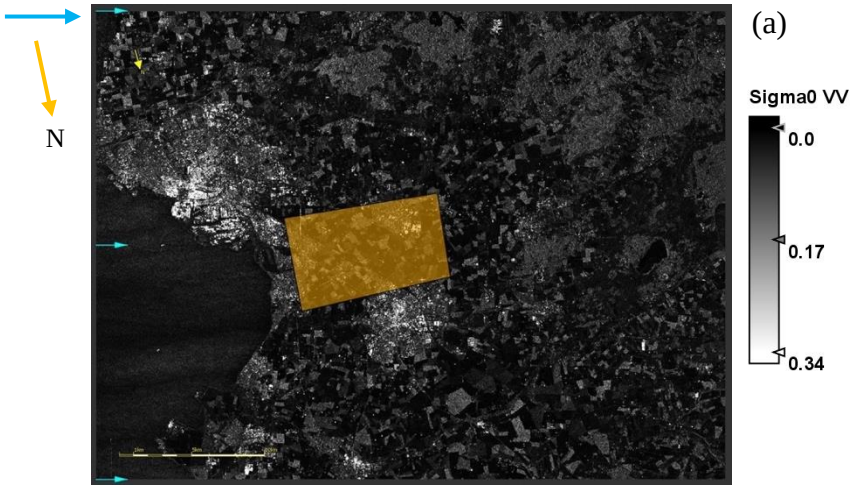

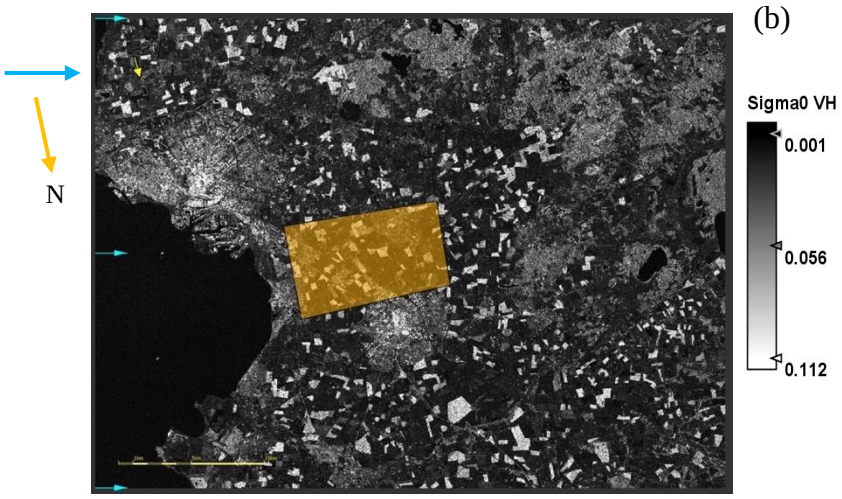

Figure 19. Radiometric calibration of S1-VV (a) and S1-VH (b)

Figure 20 shows the results of the terrain correction process for the VV (a) and VH (b) band. It can be observed how the correction of the SAR topographic distortions affects the size, orientation, and brightness (pixel value).

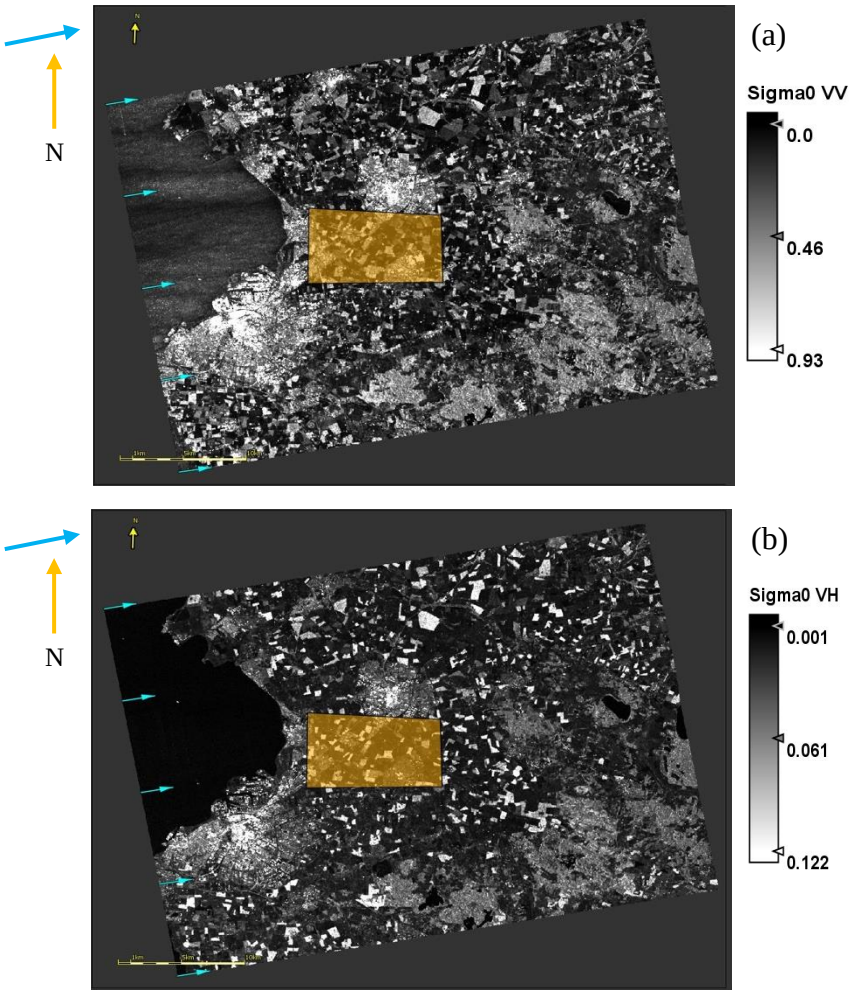

Figure 20. Terrain correction of S1-VV (a) and S1-VH (b) image.

Figure 21 shows the result of the speckle filtering process for the VV (a) and VH (b) polarizations. More homogeneous images are obtained once the random interference between the coherent returns is corrected.

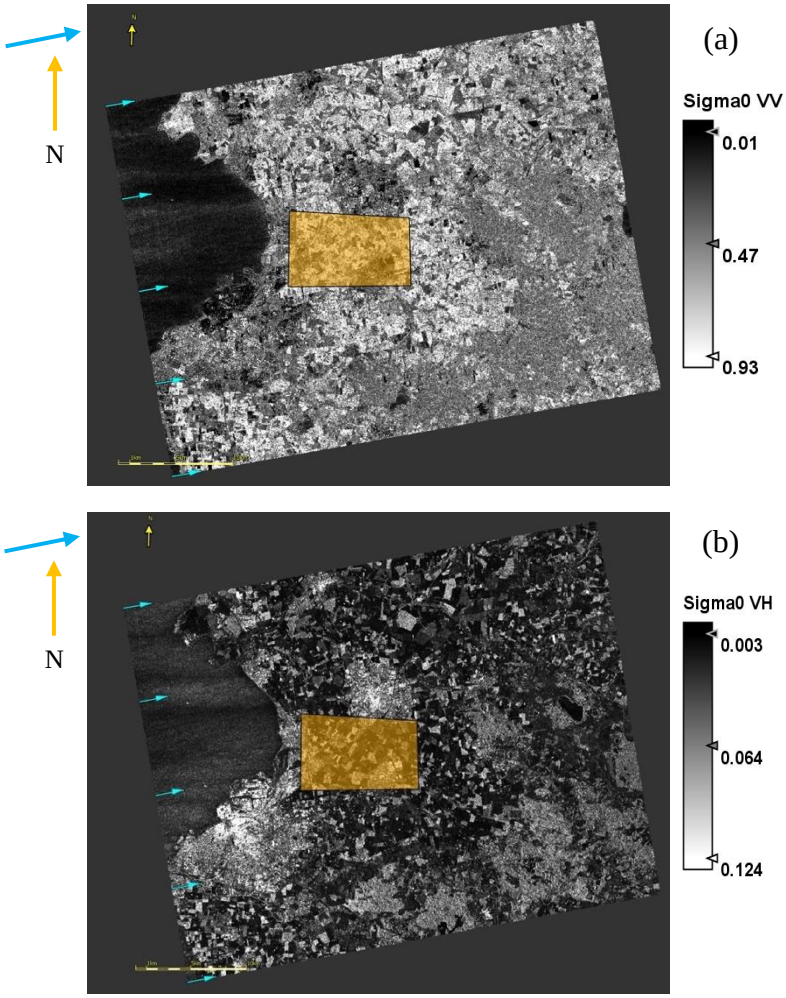

Figure 21. Sentinel-1 VV (a) and VH (b) band after the speckle filter.

Figure 22 shows the results of the VH/VV ratio. High values are represented by white colours, which means that the scattering measured on the VH polarization mode was higher than in the VV polarization mode. In opposition, low values are represented by black colours and are linked to higher scattering in the VV polarization than in the VH. The main differences are observed between forested, urban, and agricultural areas.

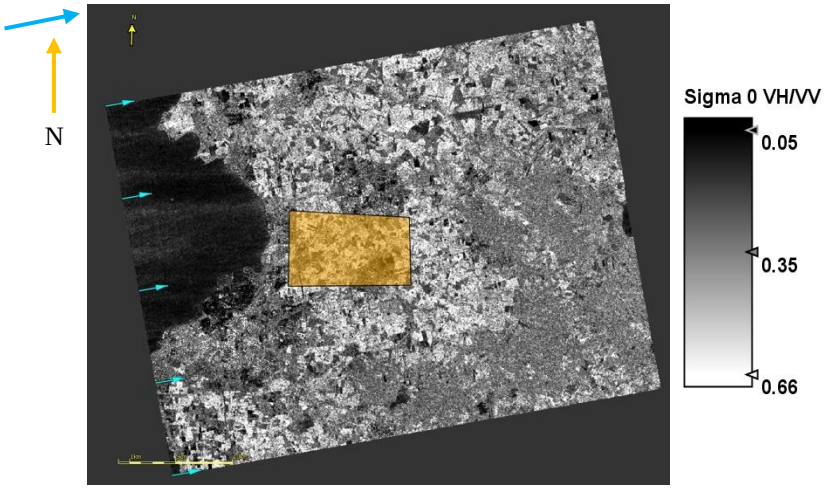

Figure 22. Ratio VH/VV calculated after the pre-processing of the Sentinel-1 product.

4.3.3 Sentinel-1 R processing

In this section, the results of the processing steps performed in R are shown. Figure 23 shows the output for the sigma (σ) VV band. It can be observed the differences between the VV scattering in urban areas and agricultural areas. Some fields present higher reflectance (white) than others (black). Figure 24 shows the result for the sigma (σ) VH band. The change of the polarization mode produces differences on the scattering of urban areas and agricultural fields. Some of them present higher reflectivity (white colour) and others are now darker.

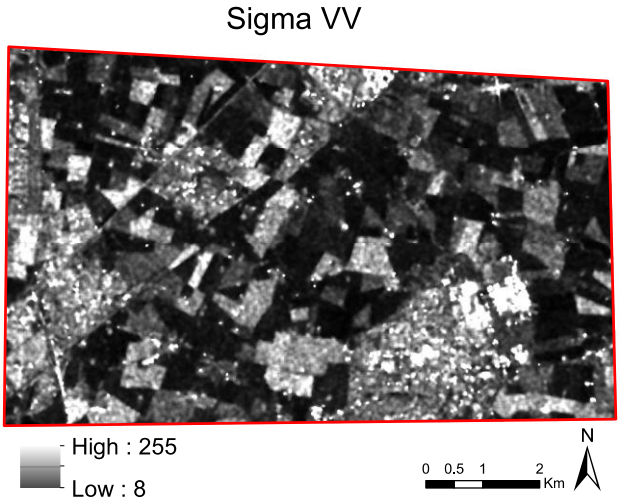

Figure 23. Sentinel-1 VV sigma (σ) band cropped to the size of the study area

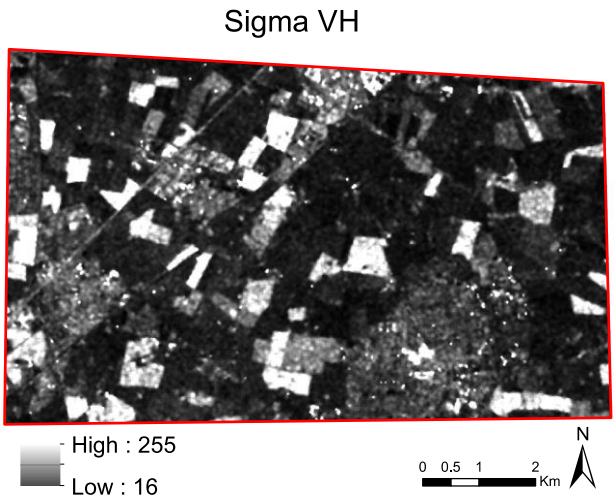

Figure 24. Sentinel-1 VH sigma (σ) band cropped to the size of the study area.

Figure 25 shows the result of the ratio VH/VV after being processed in R. As for the rest, the extent has changed to the one of the study area. In general, we can see that agricultural fields present higher values (white) than urban areas (black). The structure of the different targets (plants, buildings, etc.) is linked to the strength of the scatter radiation in both polarizations and so to the pixel value of this ratio.

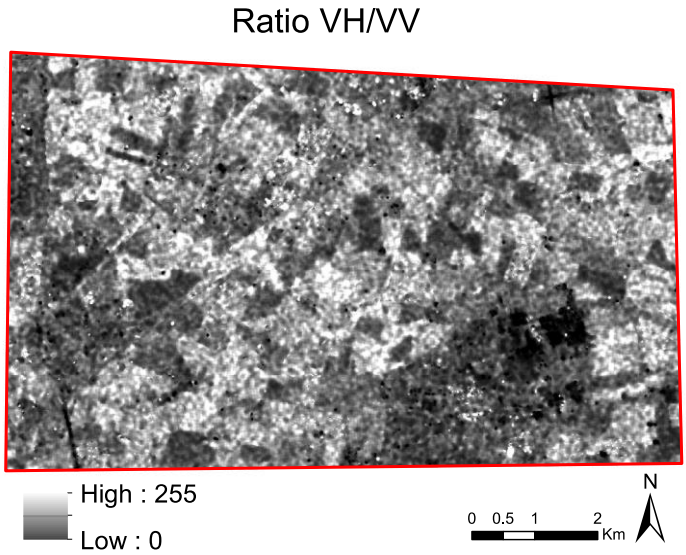

Figure 25. Ratio VH/VV cropped to the size of the study area.

4.4 Polygon based scenario

The results of the mean calculation per polygon are shown in this subsection. For the Sentinel-2 dataset, band 6 of the Sentinel-2 product used as an example is shown. For the Sentinel-1 dataset, three bands are shown. It can be observed how the use of polygons and the calculation of statistics helps to distinguish land cover class. Figure 26 shows the mean pixel value calculations per polygon for band 6. By comparing this figure with Figure 11 it can be observed that both images look similar even if the polygon based approach has been implemented.

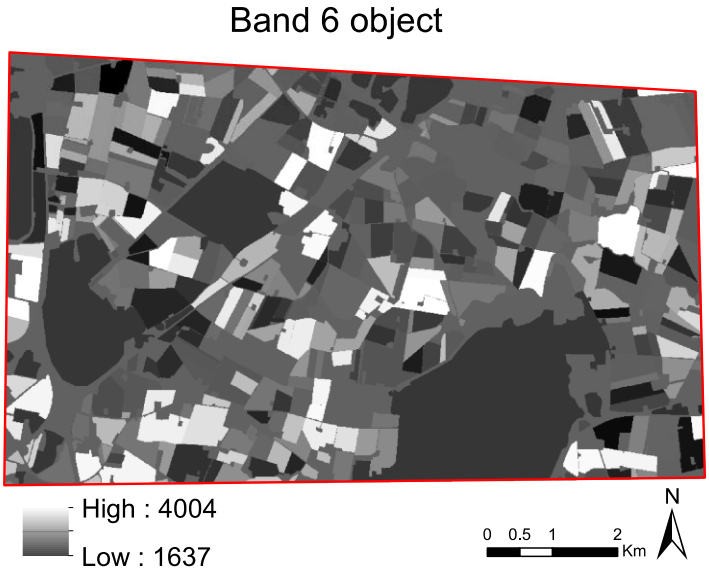

Figure 26. Mean pixel value per polygon. Values represent TOA reflectance

Figure 27 shows the mean pixel value calculation per polygon for the Sigma VH band. Comparing this image with the original (see Figure 24), the polygon based approach help to distinguish some fields from others but it also reduces the heterogeneity within each polygon.

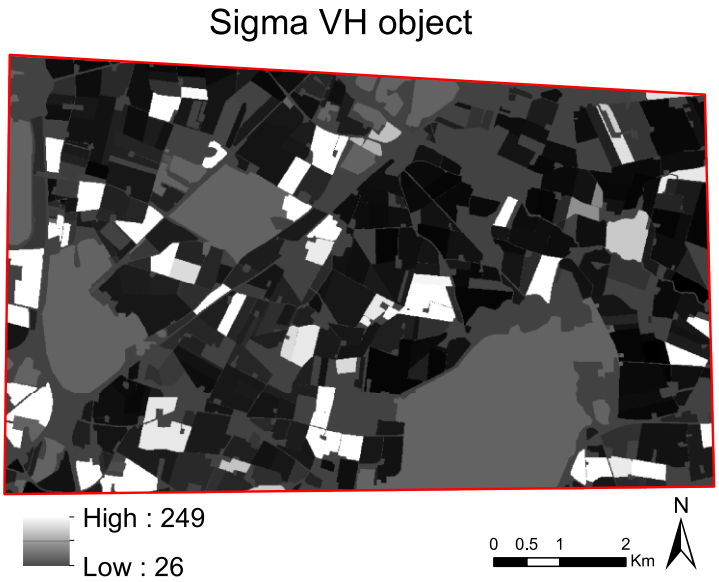

Figure 27. Mean pixel value per polygon. S1 sigma (σ) VH band

Figure 28 shows the mean pixel value calculation per polygon for the Sigma VV band. As in the previous case, the polygon based approach help to distinguish fields when comparing this image to the original one (see Figure 23)

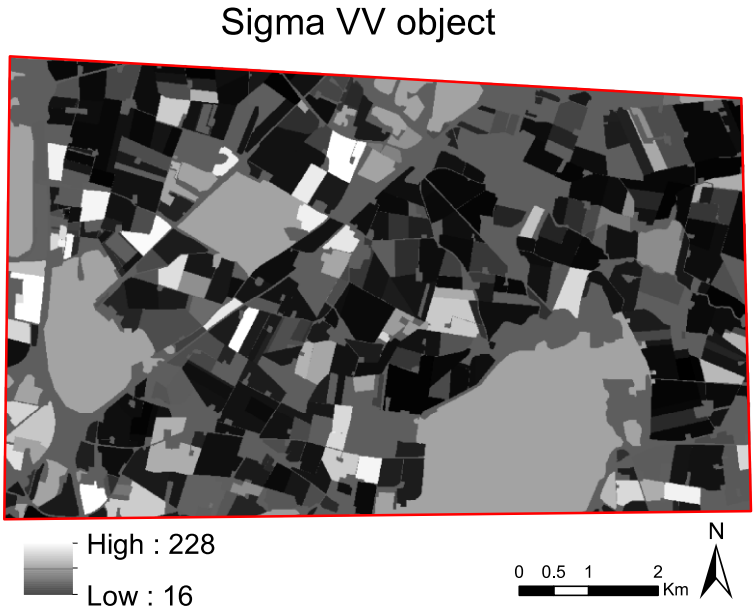

Figure 28. Mean pixel value per polygon. S1 sigma (σ) VV band.

Figure 29 shows the mean pixel value calculation per polygon. In this situation, the polygon based approach has a high impact and helps to visually interpret the image, which it is not possible in the original image (see Figure 25). Heterogeneity is reduced and polygons that could not be distinguished before are now visible.

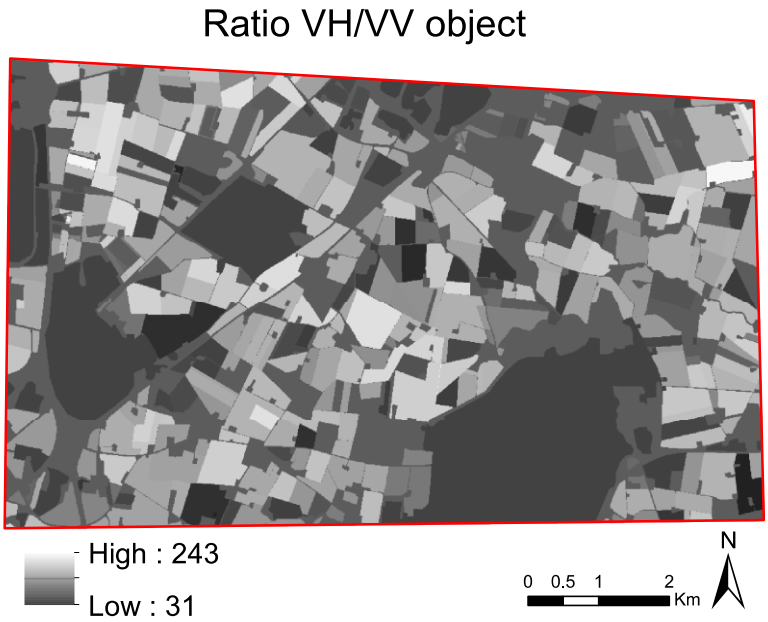

Figure 29. Mean pixel value per polygon. Ratio VH/VV.

4.5 Training and validation dataset

The training and validation datasets used in this research are shown in this section. The pattern follows a stratified random sampling approach, with 50 random points for training and 50 different random points for validation. Figure 30 shows the training points (green) and validation points (red) selected for each class.

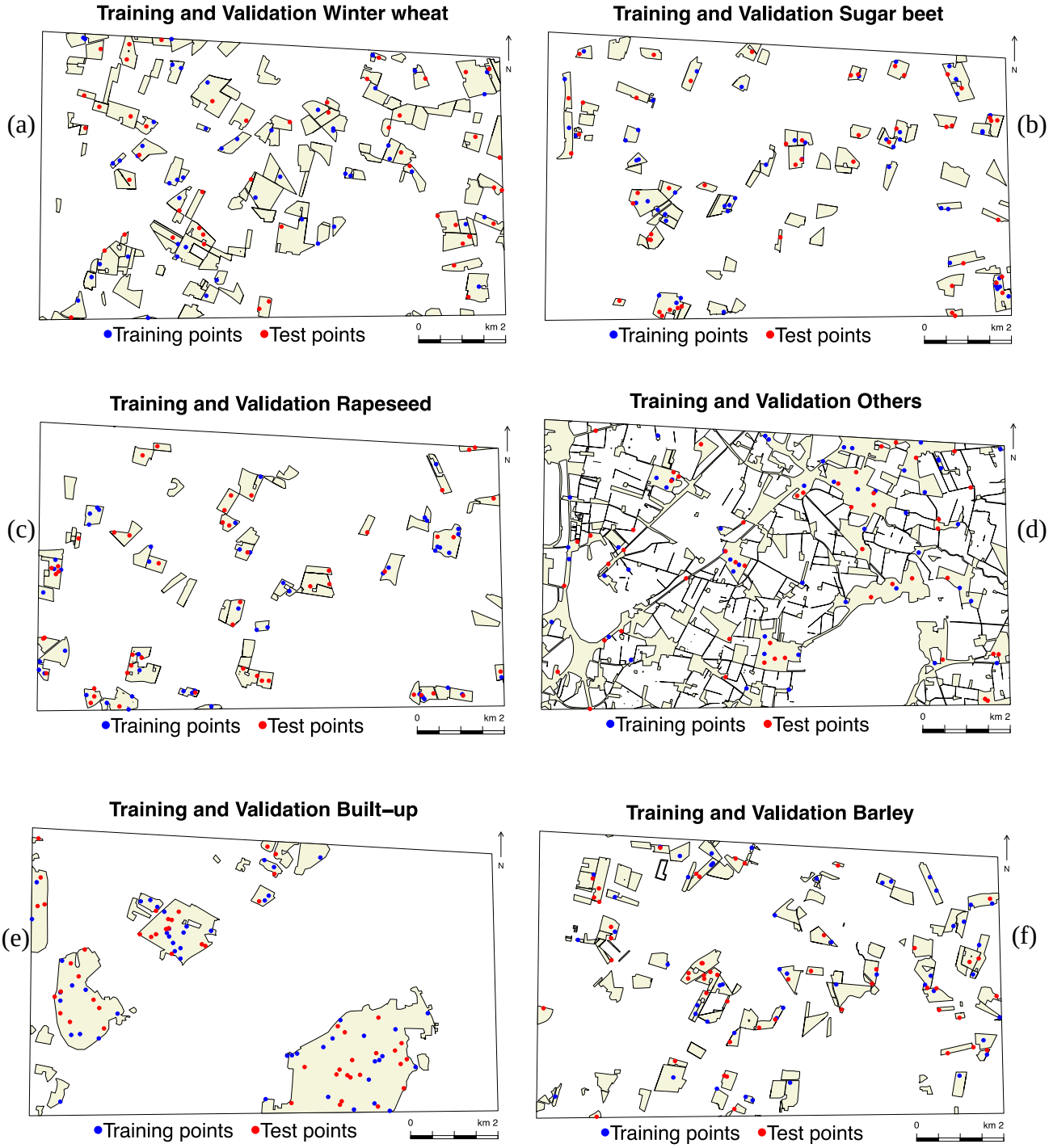

Figure 30. Training (blue) and validation (red) points per land cover: (a) Winter wheat; (b) Sugar beet; (c) Rapeseed; (d) Others; (e) Built-up; (f) Barley.

4.6 Random Forest classification pixel based

In this subsection, the results obtained with the pixel based Random Forest classification are presented. For each scenario, the result using 1 and 10/12 images are shown. The variable importance measures have been derived when using the complete dataset and are shown in Appendix II. Figure 31 shows the result of the pixel based S1 scenario using 1 image (a) and 12 (b). The classification improves considerably when adding more data.

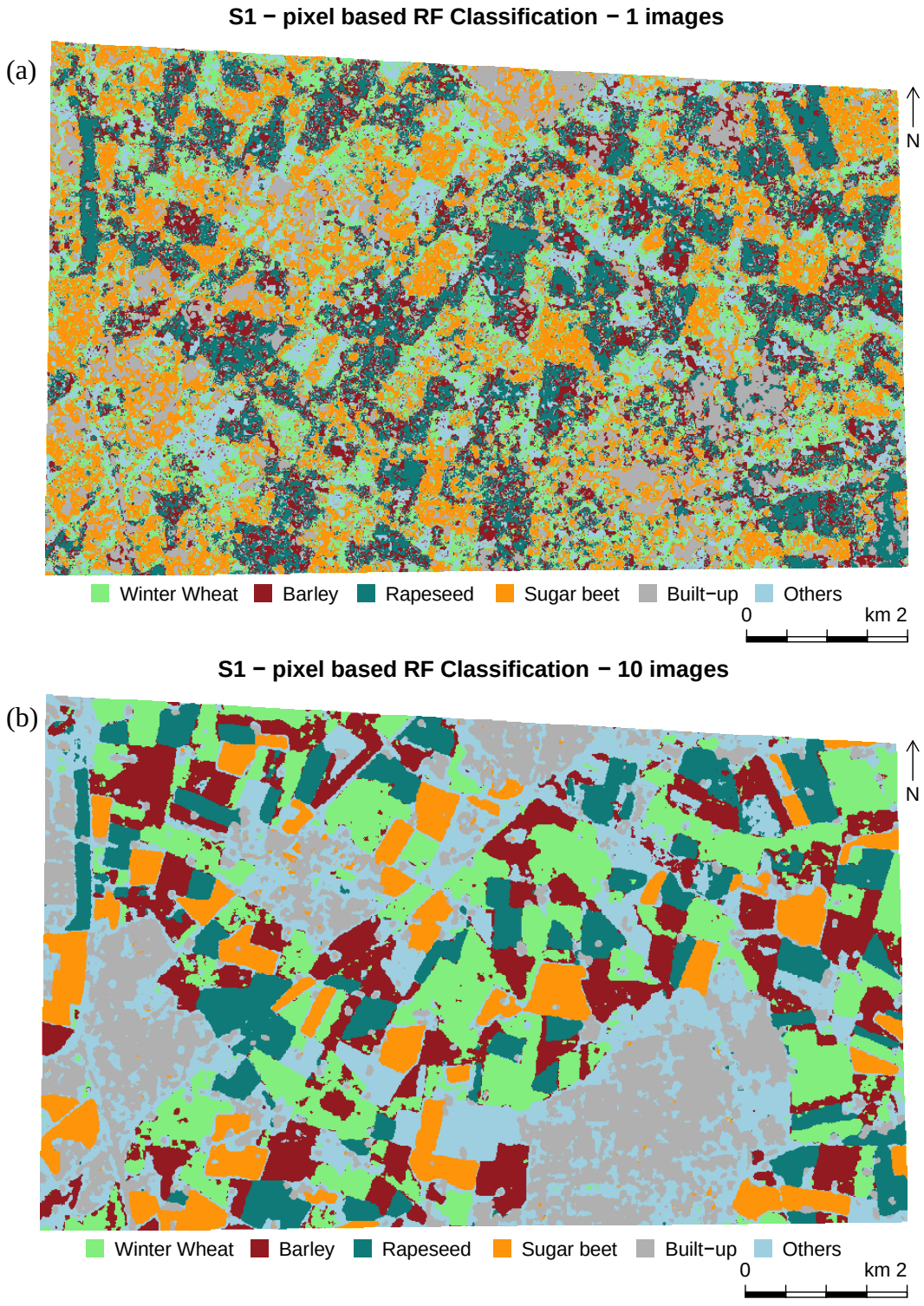

Figure 31. S1 pixel based classification. (a) uses only 1 image, (b) uses the complete dataset.

In this case, the S2 pixel based scenario is shown in Figure 32. In comparison with the S1 pixel based scenario, it can be observed that using only one image (a) already produces a better classification. Polygons are better defined and less noise is present on the image. As before, the class *Others* is barely present on the classification. When using the 12 images (b), the noise is reduced and in some areas removed. The multi-temporal approach allows us to identify the fields and the *Others* class more precisely.

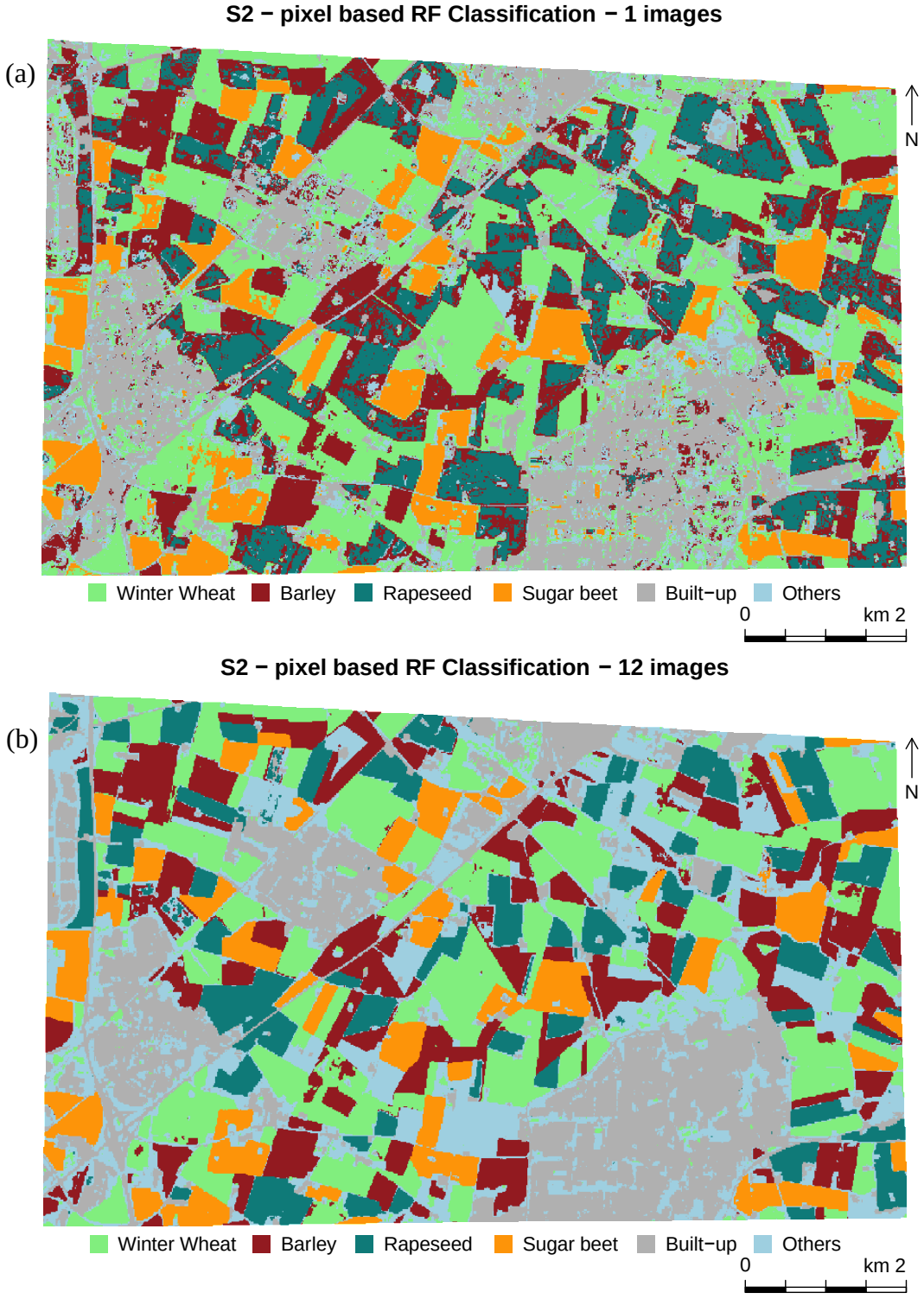

Figure 32. S2 pixel based classification. (a) uses only 1 image, (b) uses the complete dataset.

Figure 33 shows the result of the S2-VI pixel based scenario using only 1 image (a) and 12 images (b). In the first case, a similar result is obtained when combining Sentinel-2 data with vegetation indices. The same noise and misclassification of same land cover classes take place. As before when using the complete dataset, those problems are solved. It has to be highlighted that some polygons change their classification from one class to another when using 1 or 12 images. This can be observed at the bottom centre.

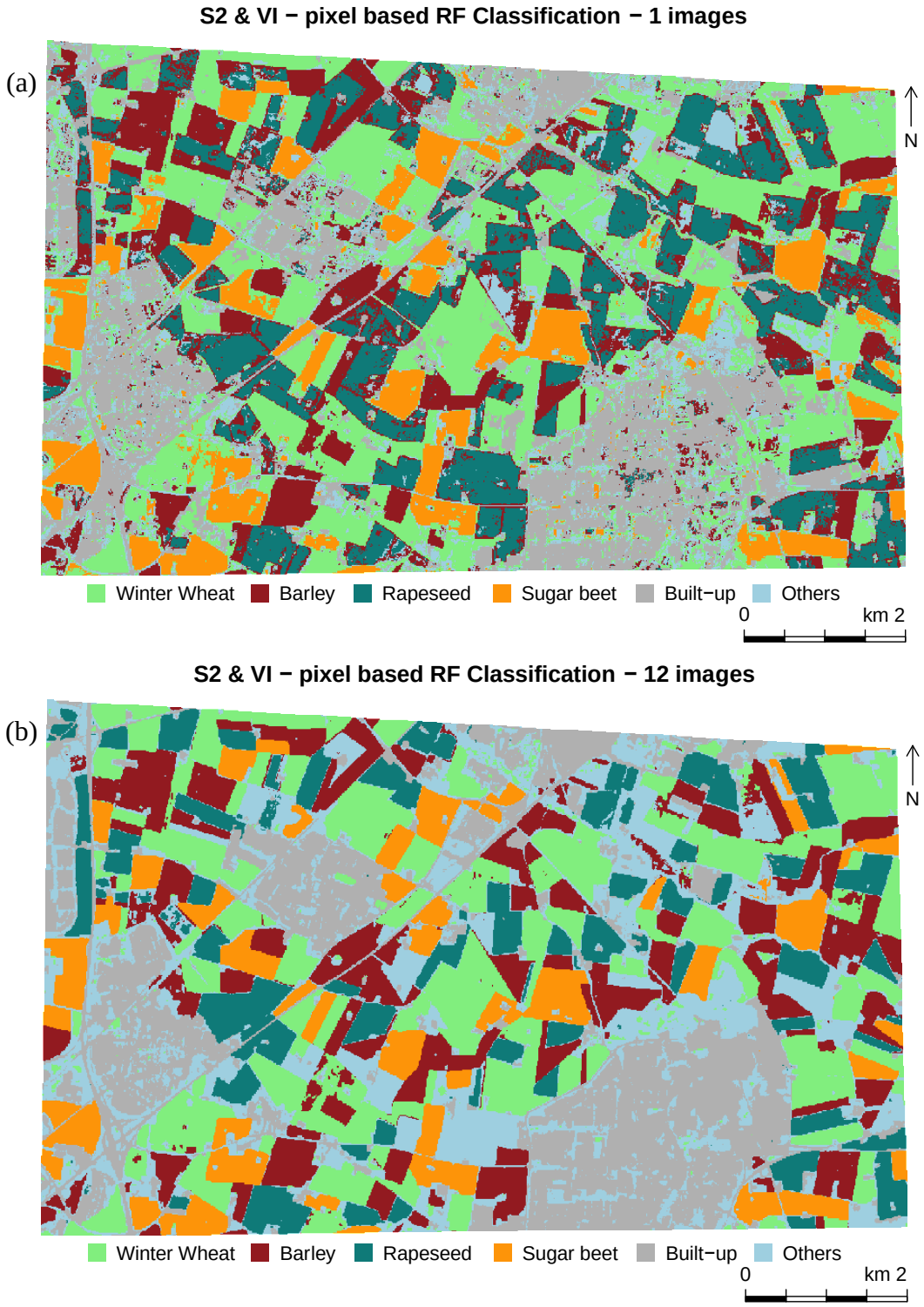

Figure 33. S2-VI pixel based classification. (a) uses only 1 image, (b) uses the complete dataset.

The last scenario of the pixel based approach, S1-S2-VI Figure 34, produces again very similar results in both cases where one image is used (a) or 12 images are used (b). The joint use of Sentinel-1, Sentinel-2, and vegetation indices produces the highest accuracy (see Table 8), but visually it is hard to distinguish any difference from the previous cases. The same distortions are found when using one image, and the same improvements are found when using 12 images.

Figure 34. S1-S2-VI pixel based classification. (a) uses only 1 image, (b) uses the complete dataset.

4.7 Random Forest classification polygon based

In this subsection, the results obtained on the Random Forest classification using the polygon based approach are presented. For each scenario, the result using 1 and 12 images are shown, except for the S1 scenarios where the complete dataset was formed by 10 images. Figure 35 shows the result of the polygon based S1 scenario using 1 image (a) and 12 (b). Although similar, some differences can be observed in the classification of some polygons when using 1 or 12 images.

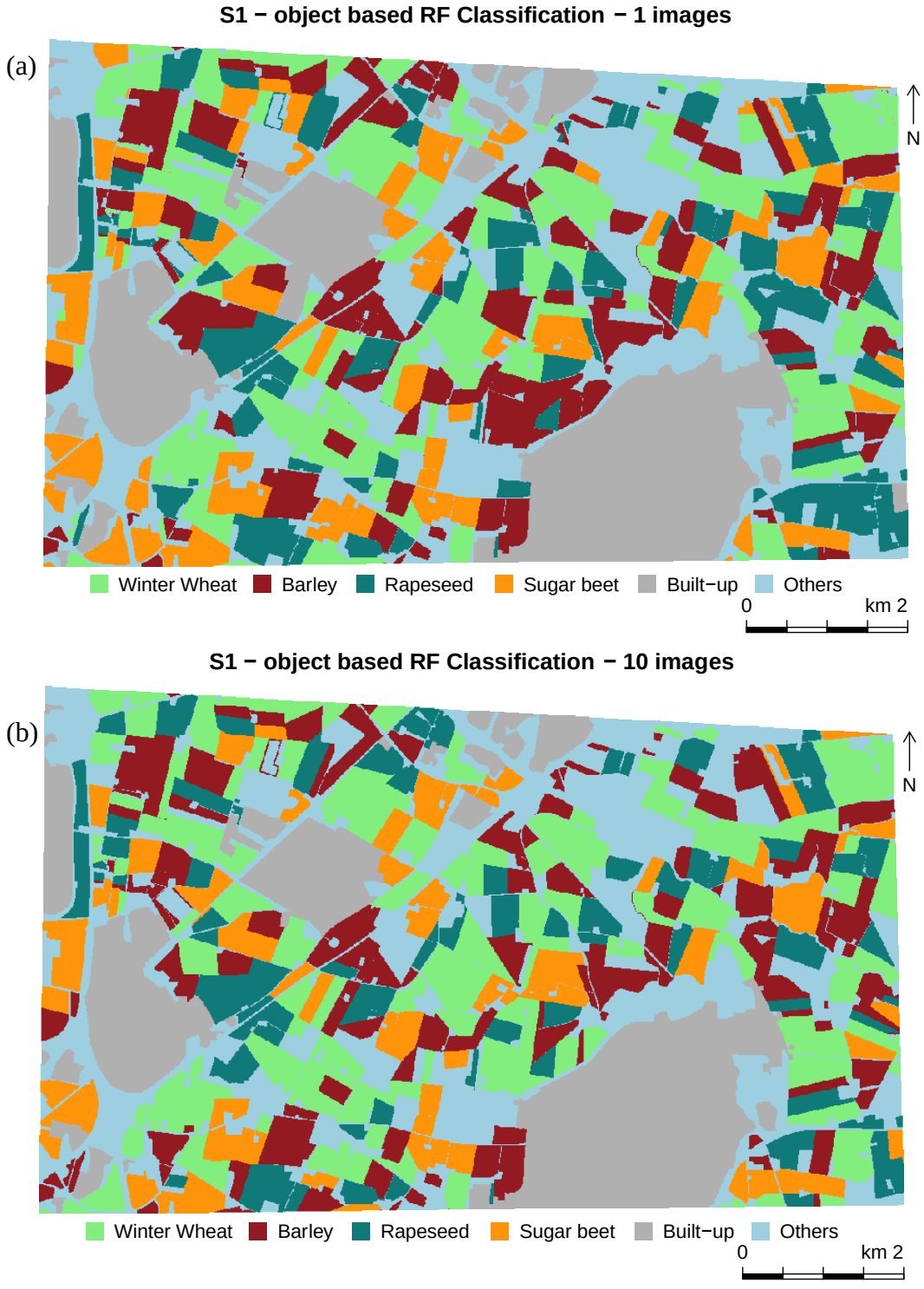

Figure 35. S1 Polygon based classification. (a) uses only 1 image, (b) uses the complete dataset.

The following case shows Figure 36, which represent the S2 polygon based scenario. A common feature of the polygon based approach is that there is no presence of the disruptions caused by using information at the pixel level. Classifications, even if using one image (a) are not affected by noise or poorly defined polygons. As before, the main difference when using a multi-temporal dataset (b) is the change in class of some polygons.

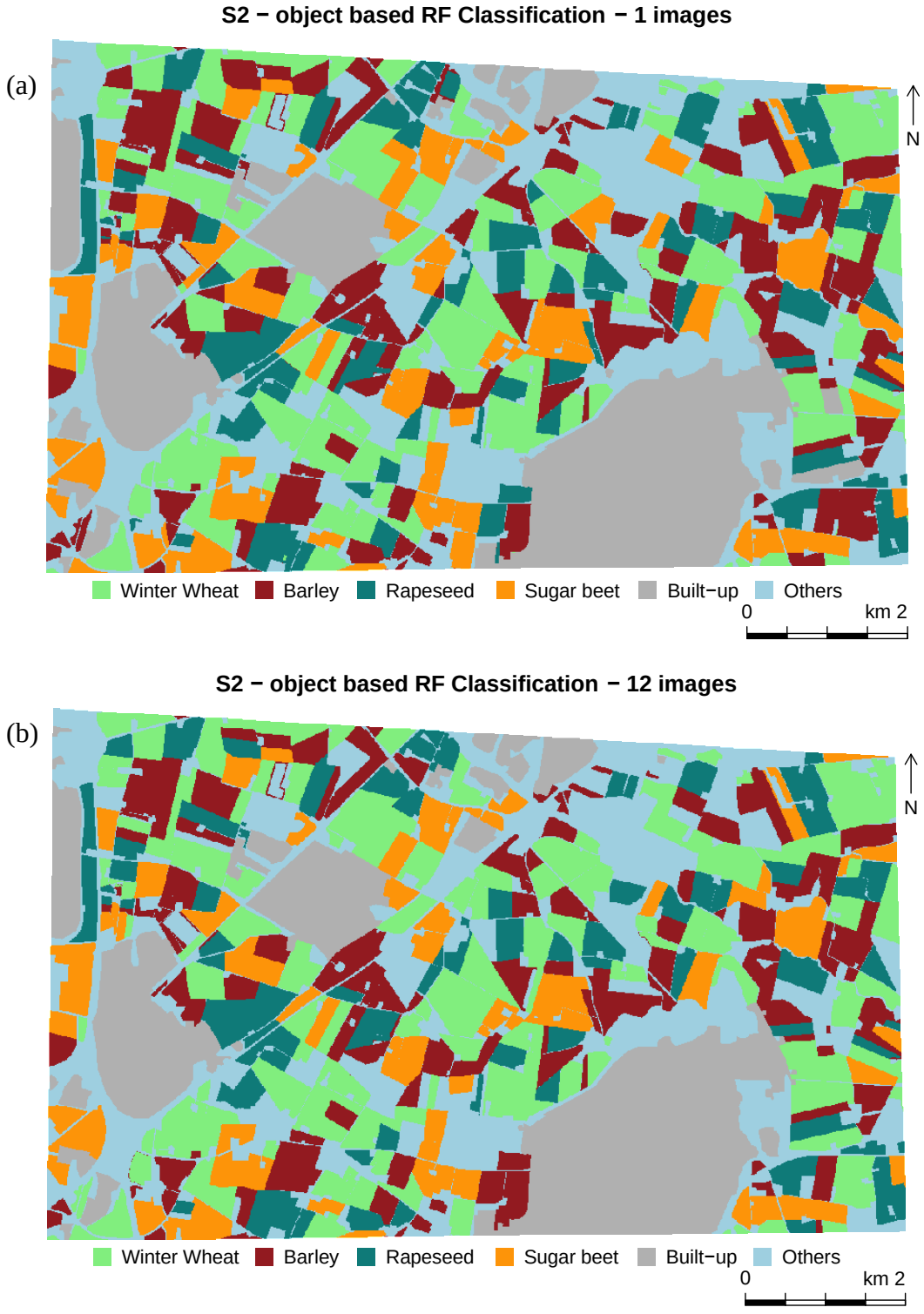

Figure 36. S2 Polygon based classification. (a) uses only 1 image, (b) uses the complete dataset.

In this page, the S2-VI polygon based scenario is shown in Figure 37. As in the S2-VI pixel based scenario, the addition of vegetation indices did not improve the classification considerably. The use of 1 image (a) and 12 images (b) produce similar results than the ones obtained in the S2 polygon based scenario (see Figure 36). The same problem of misclassification at the polygon level is found although the confusion between classes is not the same.

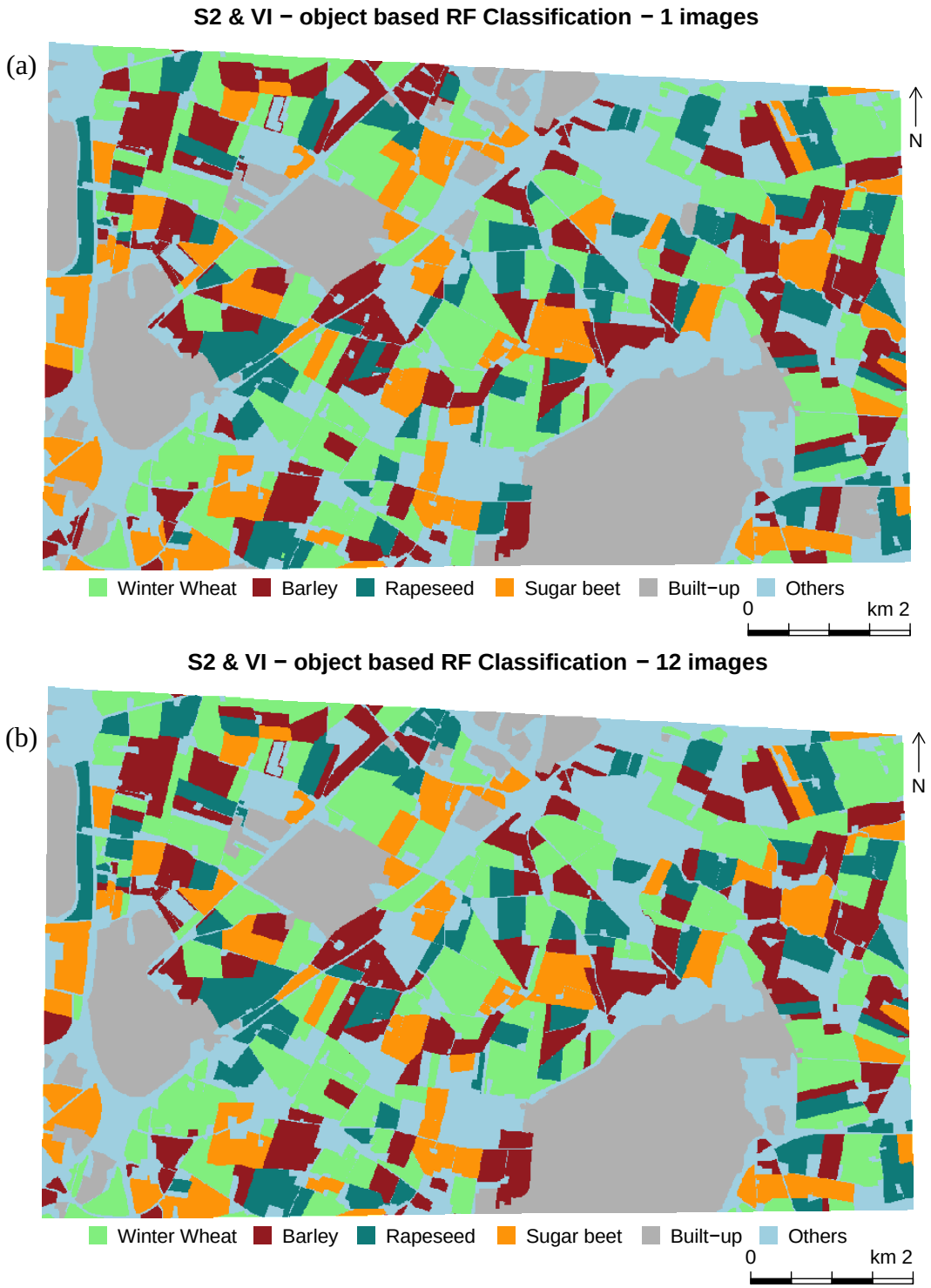

Figure 37. S2-VI Polygon based classification. (a) uses only 1 image, (b) uses the complete dataset.

Finally, Figure 38 shows the result obtained in the S1-S2-VI polygon based scenario using 1 image (a) and 12 images (b). Again, when using only 1 image, the classification falls into more inaccuracies, assigning wrong categories to some fields. The more data are added; the higher accuracies are obtained. Visually, this results only in land cover class changes, as it can be observed in the figure below.

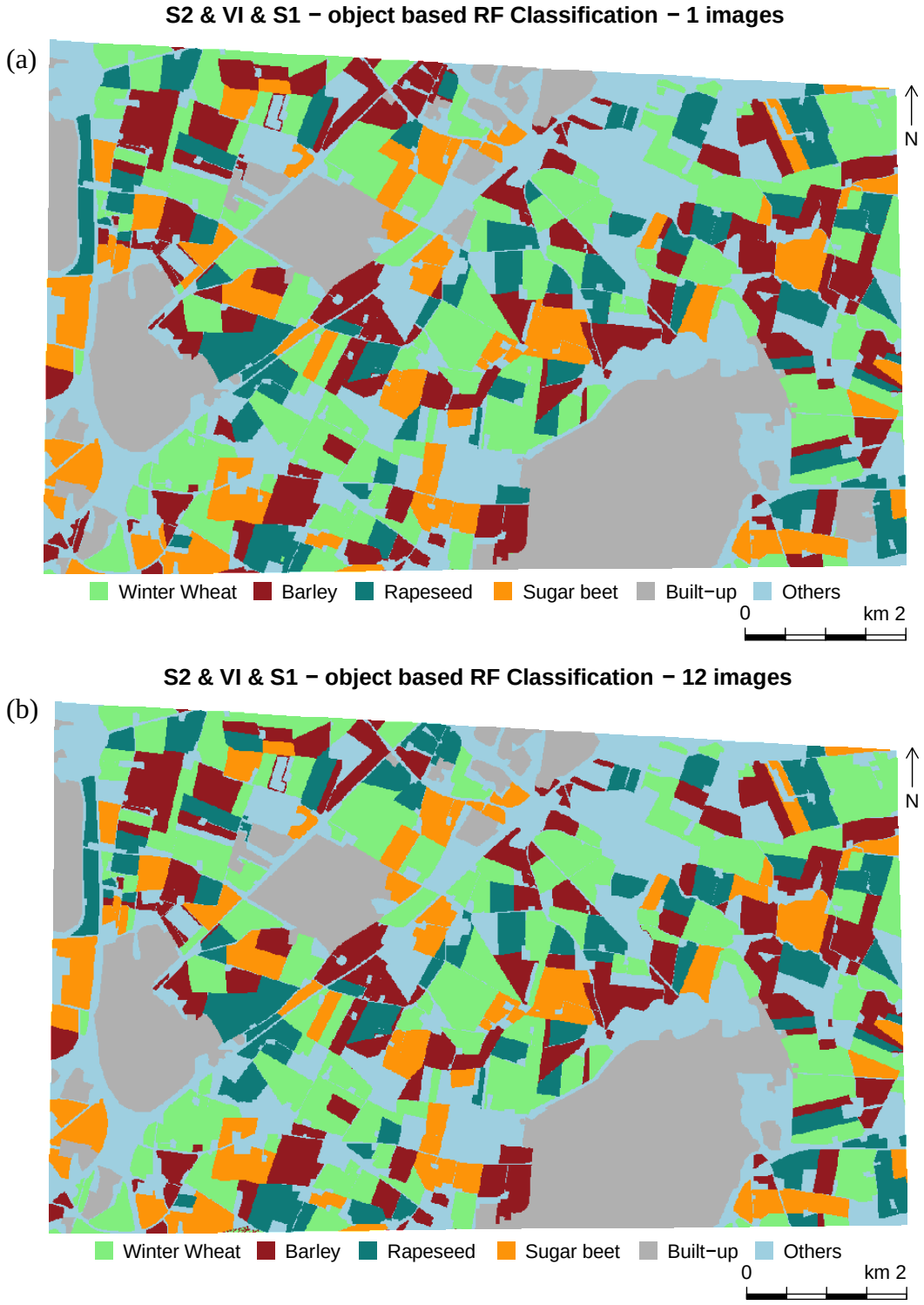

Figure 38. S1-S2-VI Polygon based classification. (a) uses only 1 image, (b) uses the complete dataset.

4.8 Accuracy evaluation

The results of the cross-validation using the complete dataset (12 images) of each scenario are presented in Table 8. The corresponding confusion matrix can be found in Appendix I. In the pixel based approach, the more data is added, the higher the accuracy values. The bigger increment is seen when joining S1, S2, and VI. Moving from the S2 scenario to the S2-VI approach, it can be seen that the increment in accuracy is very low (only 0.0067). In the polygon based approach, all the scenarios produced the same accuracy.

Table 8. Classification accuracies and kappa values per scenario.

		Accuracy	Kappa
Pixel based	S1	0.76	0.712
	S2	0.83	0.796
	S2 & VI	0.8367	0.804
	S2 & VI & S1	0.8433	0.812
Polygon based	S1	0.9867	0.984
	S2	0.9867	0.984
	S2 & VI	0.9867	0.984
	S2 & VI & S1	0.9867	0.984

Figure 39 shows the accuracies obtained for each scenario when varying the number of images used as input. The polygon based approach starts with high values of accuracies and it reaches a stability when using 4 images. Each pixel based scenario follows a different pattern, except the S1 scenario, they start and end at the same range of values.

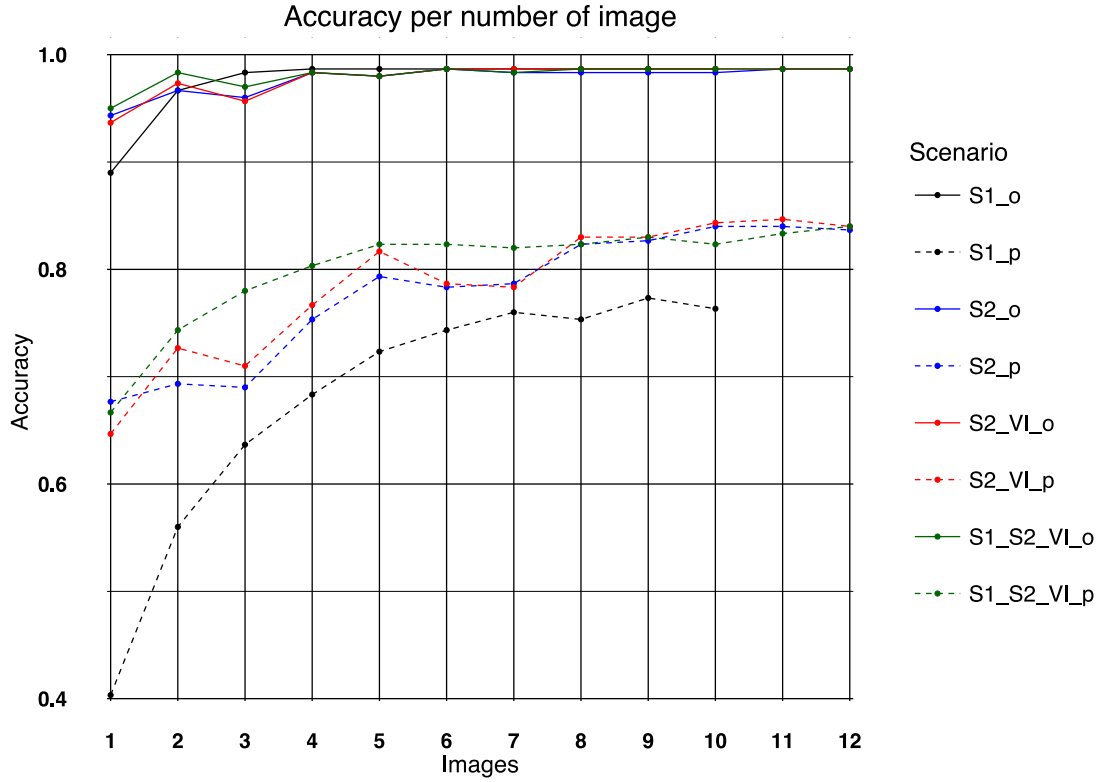

Figure 39. Accuracies per number of input images for each classification scenario. Dashed lines refer to the pixel based approach. Solid lines refer to the polygon based approach.

5 DISCUSSION

In this research, two different classification approaches (each one with four different scenarios) have been performed. The first one, pixel based, used pixel values as a source to run the process. This means that the classification model is trained using information that is not contextualized, so the resulting Random Forest model contains more noise. Due to this, the more variables are added, the more information the model can have to make decisions. The second one, polygon based, used the mean pixel value per polygon. In this section, the results are discussed and findings are explained and justified.

The pixel based approach has shown different accuracies based on the scenario. First, when running the process only with S1 images, the lowest accuracy is obtained (0.76). This can be explained by the high heterogeneity on pixel values of SAR images and the lower number of bands per image. As it can be observed in Figure 23 and Figure 24, over a field where only one crop is cultivated, SAR pixels can have high significant differences, which for a pixel based classification, represents a source of noise. This SAR feature is linked to coherent nature of SAR systems and is attributed to random interference of coherent returns issued from numerous scatters present on a surface on the scale of an image pixel (Gagnon & Jouan, 1997). These features results in wrong classification of pixels and, as it can be observed in Figure 31, in a final classification that looks less defined, with the boundaries of the fields less sharp.

Second, the Sentinel-2 scenario shows a considerable improvement of the accuracy from the previous case (0.83 vs. 0.76). Optical imagery is not affected to the same extent by the characteristic *salt-and-pepper* effect or other distortions of SAR sensors so that inside a homogeneous area, pixel values are more similar and the presence of outliers is lower. This can be observed in Figure 11, specially over agricultural fields. Having images with low variance over the same target allows the classifier to recognize classes better and produce higher accuracies. In addition, each Sentinel-2 image has 13 bands instead of the 3 bands per Sentinel-1 image. This means that the total amount of information made available for the classifier in this scenario is much higher.

Third, the use of Sentinel-2 images with vegetation indices produced a slight increment of the accuracy (0.83 to 0.8367). Adding vegetation indices as new variables for the classification was expected to improve the results, but although it did it, the increment was not very significant. This situation can be explained because vegetation indices are just an arithmetic combination of the Sentinel-2 spectral bands (see Table 3), so completely new information is not added, but just a new visualization of the same data. As an example, when comparing the vegetation index figures (Figure 13, Figure 14,

Figure 15, Figure 16) it can be observed a similar pattern for class separability (except, in this case, for the Red-Edge index –Figure 16). The same situation happened for the remaining vegetation indices derived from the rest of the Sentinel-2 images.

The fourth scenario, which combined data from both Sentinel satellites together with vegetation indices, results in the highest accuracy obtained in the pixel based approach (0.8433). Compared to the previous one (Sentinel-2 & vegetation indices), the accuracy has increased due to the contribution of the SAR sensor. In opposition to the previous case, these new variables are not related to the spectral bands of Sentinel-2, and because of that, the information is more valuable. This results in a higher accuracy increment than the one observed in the previous case (0.8367 to 0.8433).

In the pixel based approach, the main source of error was the confusion between the classes *Others* and *Built-up*, as it can be observed in the confusion matrices in the Appendix I. On one hand, the *Built-up* class covers urban areas with buildings, roads, and some parks or grasslands. On the other hand, the *Others* class is more heterogeneous and includes mainly roads and buildings but also grasslands and other crop types that have not been specifically classified. Due to the similarity between the two classes, specially because both have roads and buildings, confusion was originated. However, since the main approach of this thesis was to map agricultural fields, it has to be highlighted the low confusion between the crop classes when using the complete datasets.

In opposition to the pixel based, all the scenarios of the polygon based approach have produced the same level of accuracy (0.9867). For each scenario, the calculation of the mean pixel value per polygon of each input band removes outliers and reduce variation so that the classifier is not affected by noise in the data. The within-class variation is minimized and the between-class variation is maximized. An explanation of the high accuracies obtained in all cases is that if a polygon contains a training point, the remaining pixels will be classified correctly since they share the same pixel value as the one used for training. For each class, 50 points were randomly selected for the training set. As it can be observed in Figure 30 most of the polygons contains at least one training point which means that there will not be errors in classifying the remaining ones. The error is then produced by wrong classification of the pixels that are inside a polygon without training points. Knowing that having more than one training point per polygon does not help to better train the classifier. It only adds redundant information.

For the polygon based approach, it has to be highlighted that all the scenarios led to the same accuracy levels when using their complete dataset. However, a specific mention should be made for the scenario where only Sentinel-1 data is used. Knowing the high

percentage of cloudy days over the study area, this option allows to use remote sensing data in cloudy conditions and still be able to produce accurate land cover maps.

Another aspect to be mentioned is the use of multi-temporal data. In both approaches (pixel and polygon based) the four scenarios were tested using a progressive number of inputs, starting with one image and ending with the complete dataset of each scenario.

For the polygon based approach, using only one image led to different accuracies for each scenario. This is explained by the different number of variable the model has to be trained. The more variables used as input, the more accurate the result will be. As it can be observed in Figure 39, using one image as input, the S1-S2-VI scenario produces higher accuracy than those with only one sensor (S1 or S2). Between those, the S1 scenario is the worst due to the lower number of bands per image (3 bands per image versus 13 bands per image in S2). As soon as more images are used, the accuracies of all the scenarios increased as well, approaching a maximum value that was reached when combining four images. The drop that is observed when introducing the image 3 into the classification can be due to the presence of some clouds over the study area. The S2 and S2-VI scenarios are more affected than those containing SAR data (S1; S1-S2-VI). It can be observed that the S1 classification is not affected at all since the accuracies keep increasing.

For the pixel based approach, a similar behaviour can be found. Running the process with one image produce similar accuracies for all the scenarios except for S1 mainly because of the low number of bands per image and the heterogeneity in pixel values. Once the number of images is increased, the classifier can be trained with more data resulting in better classifications. As before, cloud presence in some images causes a drop of accuracy in the scenarios (S2; S2-VI) that do not have SAR data. In general, a maximum value is approximated when reaching 8 images. It can also be observed that the S2 and S2-VI scenarios follow a similar trend since the VI information is derived from S2. In addition, the S1-S2-VI scenario has a similar behaviour than the S1 (specially if clouds are present), but since it counts with the information from S2-VI, it reaches higher accuracies than S1.

Finally, as it can be observed from Table 8, the joint use of S1 and S2 produce the best results in the pixel based approach. Although similar values are reached by the remaining scenarios when using multi-temporal datasets, the performance of the S1-S2-VI scenario is better when having fewer images as input and in cloudy conditions. This conclusion is in line with previous studies that have investigated the join used of optical and SAR satellite imagery (Dusseux, Corpetti, Hubert-Moy, & Corgne, 2014; Hong, Zhang, Zhou, & Brisco, 2014; Inglada et al., 2016). In the case of the polygon based, the same accuracies are reached and performances with low number of images are also similar.

6 CONCLUSIONS

The pixel and polygon based classifications of specific land cover classes using multi-temporal optical and SAR remote sensing data lead to the following conclusions:

- The best accuracy (0.9867) was obtained with the polygon based approach, using the complete multi-temporal dataset and independently from the selected scenario.
- For the pixel based approach, the best accuracy (0.8433) is obtained when using the complete multi-temporal dataset of the Sentinel-1, Sentinel-2 and vegetation indices scenario.
- When combining data on the pixel based approach, the highest increment of accuracy is obtained when joining Sentinel-1 data with Sentinel-2 data and vegetation indices.
- Adding vegetation indices as variables for the pixel based classification barely improves the accuracy results.
- For the pixel and polygon based approach, Sentinel-1 data has demonstrated better performance when dealing with cloudy images.
- If multi-temporal data is available, joining images from different sensors is not mandatory to achieve high accuracy values.
- Combining SAR and optical is more relevant when dealing with a small number of input images or cloudy conditions.
- Increasing the number of images improves the accuracy but only until a certain value in which a limit is approximated.
- The benefits of joining Sentinel-1 and Sentinel-2 data are more relevant in the pixel based than in the polygon based approach

The previous conclusions of the research lead to the following recommendations:

- A new sampling schema should be tested in the polygon based approach.
- Different vegetation indices should by tested.
- Other classification algorithms should be tested to confirm the results obtained in this research.
- Since polygon based leads to the best results, a different technique, such as image segmentation, should be tested in case field boundaries are not available from a governmental organization.
- Removing images with clouds or masking them out.
- Use Sentinel-1 data to fill gaps in Sentinel-2 time-series instead of using them in combination with a maximum or minimum delay on sensing time.

7 REFERENCES

Ban, Y. (2003). Synergy of multitemporal ERS-1 SAR and Landsat TM data for classification of agricultural crops. *Canadian Journal of Remote Sensing*, *29*(4), 518–526. https://doi.org/10.5589/m03-014

Bannari, A., Morin, D., Bonn, F., & Huete, A. R. (1995). A review of vegetation indices. *Remote Sensing Reviews*, *13*(1), 95–120. https://doi.org/10.1080/02757259509532298

Bauer, M. E. (1973). Identification of agricultural crops by computer processing of ERTS-MSS data. *LARS Technical Reports. Paper 20.* Retrieved from http://docs.lib.purdue.edu/larstech/20

Becker-Reshef, I., Justice, C., Sullivan, M., Vermote, E., Tucker, C., Anyamba, A., … Doorn, B. (2010). Monitoring Global Croplands with Coarse Resolution Earth Observations: The Global Agriculture Monitoring (GLAM) Project. *Remote Sensing*, *2*(6), 1589–1609. https://doi.org/10.3390/rs2061589

Belgiu, M., & Drăgu, L. (2016). Random forest in remote sensing: A review of applications and future directions. *ISPRS Journal of Photogrammetry and Remote Sensing*, *114*, 24–31. https://doi.org/10.1016/j.isprsjprs.2016.01.011

Breiman, L. (1996). Bagging Predictors. *Machine Learning*, *24*(421), 123–140. https://doi.org/10.1007/BF00058655

Breiman, L. (2001). Random Forests. *Machine Learning*, *45*, *5–32*, *45*(1), 5–32.

Breiman, L., Friedman, J. H., Olshen, R. A., & Stone, C. J. (1984). *Classification and Regression Trees*. (W. P. Company, Ed.). Belmont, California, U.S.A.

Brisco, B., & Brown, R. J. (1995). Multidate SAR/TM synergism for crop classification in western Canada. *Photogrammetric Engineering and Remote Sensing*, *61*(8), 1009–1014. Retrieved from https://www.scopus.com/inward/record.uri?eid=2-s2.0-0028983453&partnerID=40&md5=538f78c589837a0bd2fe80d00802f545

Campus, S. B., Herrmann, I., Karnieli, A., Bonfil, D. J., Cohen, Y., & Alchanatis, V. (2010). SWIR-based spectral indices for assessing nitrogen content in potato fields. *International Journal of Remote Sensing*, *31*(19), 5127–5143. https://doi.org/10.1080/01431160903283892

Chappelle, E. W., Kim, M. S., & McMurtrey, J. E. (1992). Ratio analysis of reflectance spectra (RARS): An algorithm for the remote estimation of the concentrations of chlorophyll A, chlorophyll B, and carotenoids in soybean leaves. *Remote Sensing of Environment*, *39*(3), 239–247. https://doi.org/10.1016/0034-4257(92)90089-3

Cihlar, J. (2000). Land cover mapping of large areas from satellites: Status and research priorities. *International Journal of Remote Sensing*, *21*(6–7), 1093–1114. https://doi.org/10.1080/014311600210092

Colditz, R. R. (2015). An evaluation of different training sample allocation schemes for discrete and continuous land cover classification using decision tree-based algorithms. *Remote Sensing*, *7*(8), 9655–9681. https://doi.org/10.3390/rs70809655

Dahinden, C. (2009). An improved Random Forests approach with application to the performance prediction challenge datasets. *Hands on Pattern Recognition. Microtome*, 1–6. Retrieved from http://stat.ethz.ch/~dahinden/Paper/Bookchapter.pdf

Dash, J., Mathur, A., Foody, G. M., Curran, P. J., Chipman, J. W., & Lillesand, T. M. (2007). Land cover classification using multi-temporal MERIS vegetation indices. *International Journal of Remote Sensing*, *28*(6), 1137–1159. https://doi.org/10.1080/01431160600784259

De Wit, A. J. W., & Clevers, J. G. P. W. (2004). Efficiency and accuracy of per-field

classification for operational crop mapping. *International Journal of Remote Sensing*, *25*(20), 4091–4112. https://doi.org/10.1080/01431160310001619580

Defries, R. S., & Chan, J. C. (2000). Multiple Criteria for Evaluating Machine Learning Algorithms for Land Cover Classification from Satellite Data. *Remote Sensing and Environment*, *74*(December 2000), 503–515. https://doi.org/10.1016/S0034-4257(00)00142-5

Doraiswamy, P. C., Moulin, S., Cook, P. W., & Stern, A. (2003). Crop Yield Assessment from Remote Sensing. *Photogrammetric Engineering and Remote Sensing*, *69*(6), 665–674. https://doi.org/10.14358/PERS.69.6.665

Du, P., Samat, A., Waske, B., Liu, S., & Li, Z. (2015). Random Forest and Rotation Forest for fully polarized SAR image classification using polarimetric and spatial features. *ISPRS Journal of Photogrammetry and Remote Sensing*, *105*, 38–53. https://doi.org/http://dx.doi.org/10.1016/j.isprsjprs.2015.03.002

Dusseux, P., Corpetti, T., Hubert-Moy, L., & Corgne, S. (2014). Combined use of multi-temporal optical and Radar satellite images for grassland monitoring. *Remote Sensing*, *6*(7), 6163–6182. https://doi.org/10.3390/rs6076163

Erten, E., Lopez-Sanchez, J. M., Yuzugullu, O., & Hajnsek, I. (2016). Retrieval of agricultural crop height from space: A comparison of SAR techniques. *Remote Sensing of Environment*, *187*, 130–144. https://doi.org/10.1016/j.rse.2016.10.007

FAO. (2009). *How to Feed the World in 2050*. *Insights from an expert meeting at FAO* (Vol. 2050). https://doi.org/10.1111/j.1728-4457.2009.00312.x

Foley, J. A. (2005). Global Consequences of Land Use. *Science*, *309*(5734), 570–574. https://doi.org/10.1126/science.1111772

Fraser, R. S., Bahethi, O. P., & Al-Abbas, A. H. (1977). The effect of the atmosphere on the classification of satellite observations to identify surface features. *Remote Sensing of Environment*, *6*(3), 229–249. https://doi.org/10.1016/0034-4257(77)90005-0

Freund, Y., & Schapire, R. R. E. (1996). Experiments with a New Boosting Algorithm. *International Conference on Machine Learning*, 148–156. https://doi.org/10.1.1.133.1040

Gagnon, L., & Jouan, A. (1997). Speckle filtering of SAR images: a comparative study between complex-wavelet-based and standard filters. *Proceedings of SPIE*, *3169*, 80–91. https://doi.org/10.1117/12.279681

Gao, B. C. (1996). NDWI - A normalized difference water index for remote sensing of vegetation liquid water from space. *Remote Sensing of Environment*, *58*(3), 257–266. https://doi.org/10.1016/S0034-4257(96)00067-3

Gislason, P. O., Benediktsson, J. A., & Sveinsson, J. R. (2006). Random Forests for land cover classification. *Pattern Recognition Letters*, *27*(4), 294–300. https://doi.org/http://dx.doi.org/10.1016/j.patrec.2005.08.011

Gitelson, A. A., Keydan, G. P., & Merzlyak, M. N. (2006). Three-band model for noninvasive estimation of chlorophyll, carotenoids, and anthocyanin contents in higher plant leaves. *Geophysical Research Letters*, *33*(11), 1–6. https://doi.org/10.1029/2006GL026457

Gitelson, A. a, Gritz, Y., & Merzlyak, M. N. (2003). Relationships between leaf chlorophyll content and spectral reflectance and algorithms for non-destructive chlorophyll assessment in higher plant leaves. *Journal of Plant Physiology*, *160*(3), 271–82. https://doi.org/10.1078/0176-1617-00887

Gómez, C., White, J. C., & Wulder, M. A. (2016). Optical remotely sensed time series data for land cover classification: A review. *ISPRS Journal of Photogrammetry and Remote Sensing*, *116*, 55–72. https://doi.org/10.1016/j.isprsjprs.2016.03.008

Haack, B., & Bechdol, M. (2000). Integrating multisensor data and RADAR texture measures for land cover mapping. *Computers and Geosciences*, *26*(4), 411–421. https://doi.org/10.1016/S0098-3004(99)00121-1

Hirooka, Y., Homma, K., Maki, M., & Sekiguchi, K. (2015). Applicability of synthetic aperture radar (SAR) to evaluate leaf area index (LAI) and its growth rate of rice in farmers' fields in Lao PDR. *Field Crops Research*, *176*, 119–122. https://doi.org/10.1016/j.fcr.2015.02.022

Hong, G., Zhang, A., Zhou, F., & Brisco, B. (2014). Integration of optical and synthetic aperture radar (SAR) images to differentiate grassland and alfalfa in Prairie area. *International Journal of Applied Earth Observation and Geoinformation*, *28*(1), 12–19. https://doi.org/10.1016/j.jag.2013.10.003

Inglada, J., Vincent, A., Arias, M., & Marais-Sicre, C. (2016). Improved early crop type identification by joint use of high temporal resolution sar and optical image time series. *Remote Sensing*, *8*(5). https://doi.org/10.3390/rs8050362

Jiang, Z., Huete, A. R., Didan, K., & Miura, T. (2008). Development of a two-band enhanced vegetation index without a blue band. *Remote Sensing of Environment*, *112*(10), 3833–3845. https://doi.org/10.1016/j.rse.2008.06.006

Lawrence, R. L., Wood, S. D., & Sheley, R. L. (2006). Mapping invasive plants using hyperspectral imagery and Breiman Cutler classifications (randomForest). *Remote Sensing of Environment*, *100*(3), 356–362. https://doi.org/https://doi.org/10.1016/j.rse.2005.10.014

Lee, J. S., Wen, J. H., Ainsworth, T. L., Chen, K. S., & Chen, A. J. (2009). Improved Sigma Filter for Speckle Filtering of SAR Imagery. *IEEE Transactions on Geoscience and Remote Sensing*. https://doi.org/10.1109/TGRS.2008.2002881

Liaw, a, & Wiener, M. (2002). Classification and Regression by randomForest. *R News*, *2*(December), 18–22. https://doi.org/10.1177/154405910408300516

McNairn, H., Champagne, C., Shang, J., Holmstrom, D., & Reichert, G. (2009). Integration of optical and Synthetic Aperture Radar (SAR) imagery for delivering operational annual crop inventories. *ISPRS Journal of Photogrammetry and Remote Sensing*, *64*(5), 434–449. https://doi.org/10.1016/j.isprsjprs.2008.07.006

Meenakshi, a V, & Punitham, V. (2011). Performance of Speckle Noise Reduction Filters on Active Radar and SAR Images. *International Journal of Technology And Engineering System (IJTES)*, *2*(1), 111–114.

Moran, M. S., Alonso, L., Moreno, J. F., Pilar Cendrero Mateo, M., de la Cruz, D., & Montoro, A. (2012). A {RADARSAT-2} Quad-Polarized Time Series for Monitoring Crop and Soil Conditions in {B}arrax, {S}pain, *50*(4), 1057–1070. https://doi.org/10.1109/TGRS.2011.2166080

Mróz, M., & Sobieraj, A. (2004). Comparison of several vegetation indices calculated on the basis of a seasonal SPOT XS time series, and their suitability for land cover and agricultural crop identification. *Technical Sciences*, *7*(7), 39–66. https://doi.org/10.1080/10106040608542399

Mulla, D. J. (2013). Twenty five years of remote sensing in precision agriculture: Key advances and remaining knowledge gaps. *Biosystems Engineering*, *114*(4), 358–371. https://doi.org/10.1016/j.biosystemseng.2012.08.009

Pohl, C., & Van Genderen, J. L. (1998). Review article Multisensor image fusion in remote sensing: Concepts, methods and applications. *International Journal of Remote Sensing*, *19*(5), 823–854. https://doi.org/10.1080/014311698215748

Potter, J. F. (1974). Haze And Sun Angle Effects On Automatic Classification Of Satellite Data-Simulation And Correction. In *Photo-Opt. Instrum. Eng.* (Vol. 51, pp. 73–83). Retrieved from http://dx.doi.org/10.1117/12.964562

Prasad, A. K., Chai, L., Singh, R. P., & Kafatos, M. (2006). Crop yield estimation model for Iowa using remote sensing and surface parameters. *International Journal of Applied Earth Observation and Geoinformation*, *8*(1), 26–33. https://doi.org/10.1016/j.jag.2005.06.002

Rodriguez-Galiano, V. F., Ghimire, B., Rogan, J., Chica-Olmo, M., & Rigol-Sanchez, J. P. (2012). An assessment of the effectiveness of a random forest classifier for land-cover classification. *ISPRS Journal of Photogrammetry and Remote Sensing*, *67*, 93–104. https://doi.org/http://dx.doi.org/10.1016/j.isprsjprs.2011.11.002

Rogan, J., & Chen, D. (2004). Remote sensing technology for mapping and monitoring land-cover and land-use change. *Progress in Planning*, *61*(4), 301–325. https://doi.org/10.1007/s10708-004-4936-0

Rouse, W., Haas, R. H., Schell, J. A., & Deering, D. W. (1974). Monitoring vegetation systems in the Great Plains with ERTS. *Proceedings of the Third Earth Resources Technology Satellite- 1 Symposium*, 301–317.

Solberg, A. H. S., Jain, A. K., & Taxt, T. (1994). Multisource classification of remotely sensed data: fusion of Landsat TM and SAR images. *IEEE Transactions on Geoscience and Remote Sensing*. https://doi.org/10.1109/36.298006

Song, C., Woodcock, C. E., Seto, K. C., Lenney, M. P., & Macomber, S. A. (2001). Classification and change detection using Landsat TM data: When and how to correct atmospheric effects? *Remote Sensing of Environment*, *75*(2), 230–244. https://doi.org/10.1016/S0034-4257(00)00169-3

Song, X.-P., Potapov, P. V, Krylov, A., King, L., Di Bella, C. M., Hudson, A., … Hansen, M. C. (2017). National-scale soybean mapping and area estimation in the United States using medium resolution satellite imagery and field survey. *Remote Sensing of Environment*, *190*, 383–395. https://doi.org/10.1016/j.rse.2017.01.008

Stefanski, J., Mack, B., & Waske, B. (2013). Optimization of Object-Based Image Analysis With Random Forests for Land Cover Mapping. *IEEE Journal of Selected Topics in Applied Earth Observations and Remote Sensing*. https://doi.org/10.1109/JSTARS.2013.2253089

Townshend, J., Justice, C., Li, W., Gurney, C., & McManus, J. (1991). Global land cover classification by remote sensing: present capabilities and future possibilities. *Remote Sensing of Environment*, *35*(2–3), 243–255. https://doi.org/10.1016/0034-4257(91)90016-Y

Watts, J. D., Powell, S. L., Lawrence, R. L., & Hilker, T. (2011). Improved classification of conservation tillage adoption using high temporal and synthetic satellite imagery. *Remote Sensing of Environment*, *115*(1), 66–75. https://doi.org/10.1016/j.rse.2010.08.005

Wegener, S. (2001). *Remote Sensing Technology Trends and Agriculture*. Retrieved from https://dg-cms-uploads-production.s3.amazonaws.com/uploads/document/file/31/DG-RemoteSensing-WP.pdf

Wojtowicz, M., Wojtowics, A., & Piekarczyk, J. (2015). Application of remote sensing methods in Agriculture. *Communication in Biometry and Crop Science*, *11*(1), 31–50.

APPENDIX I

The following tables show the confusion matrices obtained for each Random Forest classification scenario when using their corresponding complete dataset.

Confusion Matrix S1 pixel based

CM S1 pixel		Reference							
		Barley	Others	Rapeseed	Sugar beet	Built-up	Winter Wheat	Totals	User's Accuracy
Prediction	Barley	44	4	0	1	0	8	57	77%
	Others	4	30	5	0	19	6	64	46%
	Rapeseed	0	2	44	0	0	0	46	95%
	Sugar beet	2	1	0	49	0	2	54	90%
	Built-up	0	12	1	0	31	0	44	70%
	Winter Wheat	0	1	0	0	0	34	35	97%
Totals		50	50	50	50	50	50	300	
Producer's Accuracy		88%	60%	88%	98%	62%	68%		

Confusion Matrix S2 pixel based

CM S2 pixel		Reference							
		Barley	Others	Rapeseed	Sugar beet	Built-up	Winter Wheat	Totals	User's Accuracy
Prediction	Barley	44	1	0	2	0	5	52	84%
	Others	4	35	4	1	8	3	55	63%
	Rapeseed	0	1	46	0	0	0	47	98%
	Sugar beet	2	0	0	47	0	0	49	96%
	Built-up	0	10	0	0	41	2	53	77%
	Winter Wheat	0	3	0	0	1	40	44	91%
Totals		50	50	50	50	50	50	300	
Producer's Accuracy		88%	70%	92%	94%	82%	80%		

Confusion Matrix S2-VI pixel based

CM S2-VI pixel		Reference							
		Barley	Others	Rapeseed	Sugar beet	Built-up	Winter Wheat	Totals	User's Accuracy
Prediction	Barley	44	2	0	1	0	7	54	81%
	Others	4	33	2	2	9	1	51	65%
	Rapeseed	0	1	47	0	0	0	48	98%
	Sugar beet	2	0	0	47	0	0	49	96%
	Built-up	0	13	0	0	40	2	55	73%
	Winter Wheat	0	1	1	0	1	40	43	93%
Totals		50	50	50	50	50	50	300	
Producer's Accuracy		88%	66%	94%	94%	80%	80%		

Confusion Matrix S1-S2-VI pixel based

CM S1-S2-VI pixel		Reference							
		Barley	Others	Rapeseed	Sugar beet	Built-up	Winter Wheat	Totals	User's Accuracy
Prediction	Barley	44	2	0	1	0	7	54	81%
	Others	4	38	2	2	15	3	64	59%
	Rapeseed	0	2	47	0	0	0	49	96%
	Sugar beet	2	0	0	47	0	0	49	96%
	Built-up	0	8	1	0	35	1	45	78%
	Winter Wheat	0	0	0	0	0	39	39	100%
Totals		50	50	50	50	50	50	300	
Producer's Accuracy		88%	76%	94%	94%	70%	78%		

Confusion Matrix S1 polygon based

CM S1 polygon		Reference							
		Barley	Others	Rapeseed	Sugar beet	Built-up	Winter Wheat	Totals	User's Accuracy
Prediction	Barley	49	0	0	1	0	3	53	92%
	Others	1	50	0	0	0	0	51	98%
	Rapeseed	0	0	50	0	0	0	50	100%
	Sugar beet	0	0	0	49	0	0	49	100%
	Built-up	0	0	0	0	50	0	50	100%
	Winter Wheat	0	0	0	0	0	47	47	100%
Totals		50	50	50	50	50	50	300	
Producer's Accuracy		98%	100%	100%	98%	100%	94%		

Confusion Matrix S2 polygon based

CM S2 polygon		Reference							
		Barley	Others	Rapeseed	Sugar beet	Built-up	Winter Wheat	Totals	User's Accuracy
Prediction	Barley	48	0	0	1	0	2	51	94%
	Others	0	50	0	0	0	0	50	100%
	Rapeseed	0	0	50	0	0	0	50	100%
	Sugar beet	0	0	0	49	0	0	49	100%
	Built-up	0	0	0	0	50	0	50	100%
	Winter Wheat	2	0	0	0	0	48	50	96%
Totals		50	50	50	50	50	50	300	
Producer's Accuracy		96%	100%	100%	98%	100%	96%		

Confusion Matrix S2-VI polygon based

CM S2-VI polygon		Reference							
		Barley	Others	Rapeseed	Sugar beet	Built-up	Winter Wheat	Totals	User's Accuracy
Prediction	Barley	48	0	0	1	0	2	51	94%
	Others	0	50	0	0	0	0	50	100%
	Rapeseed	0	0	50	0	0	0	50	100%
	Sugar beet	0	0	0	49	0	0	49	100%
	Built-up	0	0	0	0	50	0	50	100%
	Winter Wheat	2	0	0	0	0	48	50	96%
Totals		50	50	50	50	50	50	300	
Producer's Accuracy		96%	100%	100%	98%	100%	96%		

Confusion Matrix S1-S2-VI polygon based

CM S1-S2-VI polygon		Reference							
		Barley	Others	Rapeseed	Sugar beet	Built-up	Winter Wheat	Totals	User's Accuracy
Prediction	Barley	48	0	0	1	0	1	50	96%
	Others	0	50	0	0	0	0	50	100%
	Rapeseed	0	0	50	0	0	0	50	100%
	Sugar beet	0	0	0	49	0	0	49	100%
	Built-up	0	0	0	0	50	0	50	100%
	Winter Wheat	2	0	0	0	0	49	51	96%
Totals		50	50	50	50	50	50	300	
Producer's Accuracy		96%	100%	100%	98%	100%	98%		

APPENDIX II

The following figures show the variable importance measurements: Mean Decrease in GINI (MDG) and Mean Decrease in Accuracy (MDA). They are obtained for each Random Forest classification scenario when using their corresponding complete dataset.

Variable Importance RF S1 pixel based

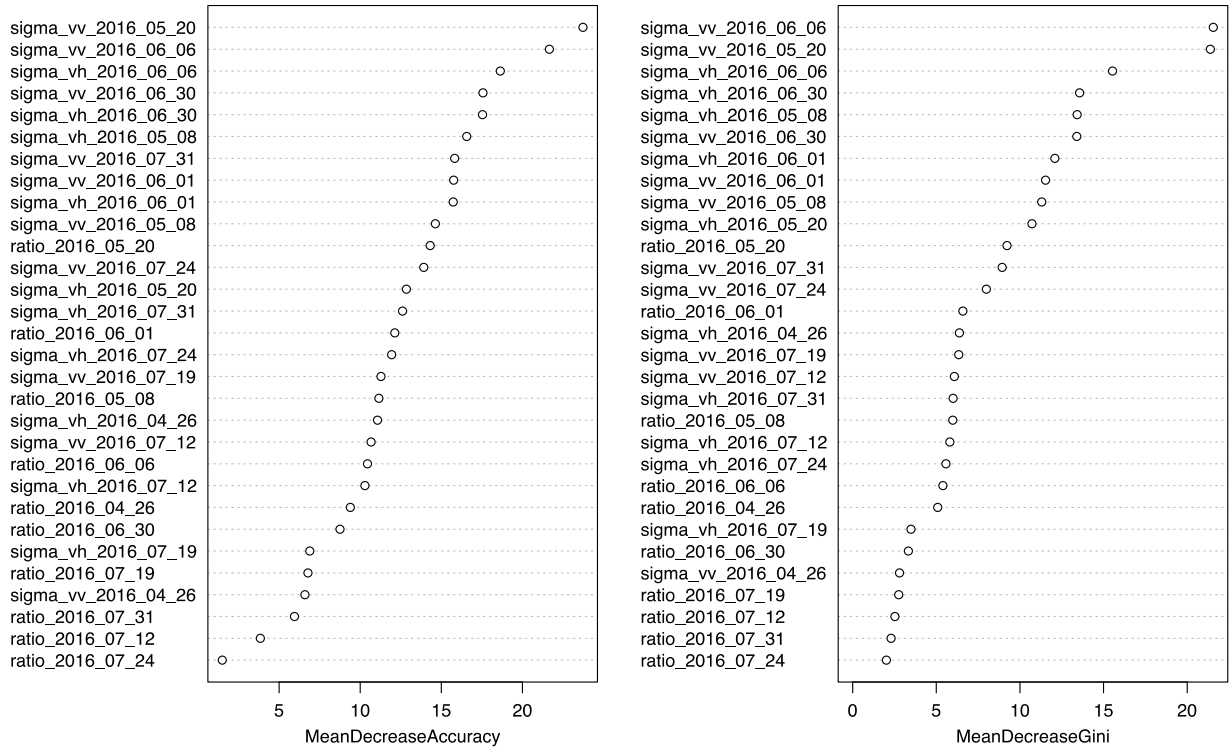

Variable Importance RF S2 pixel based

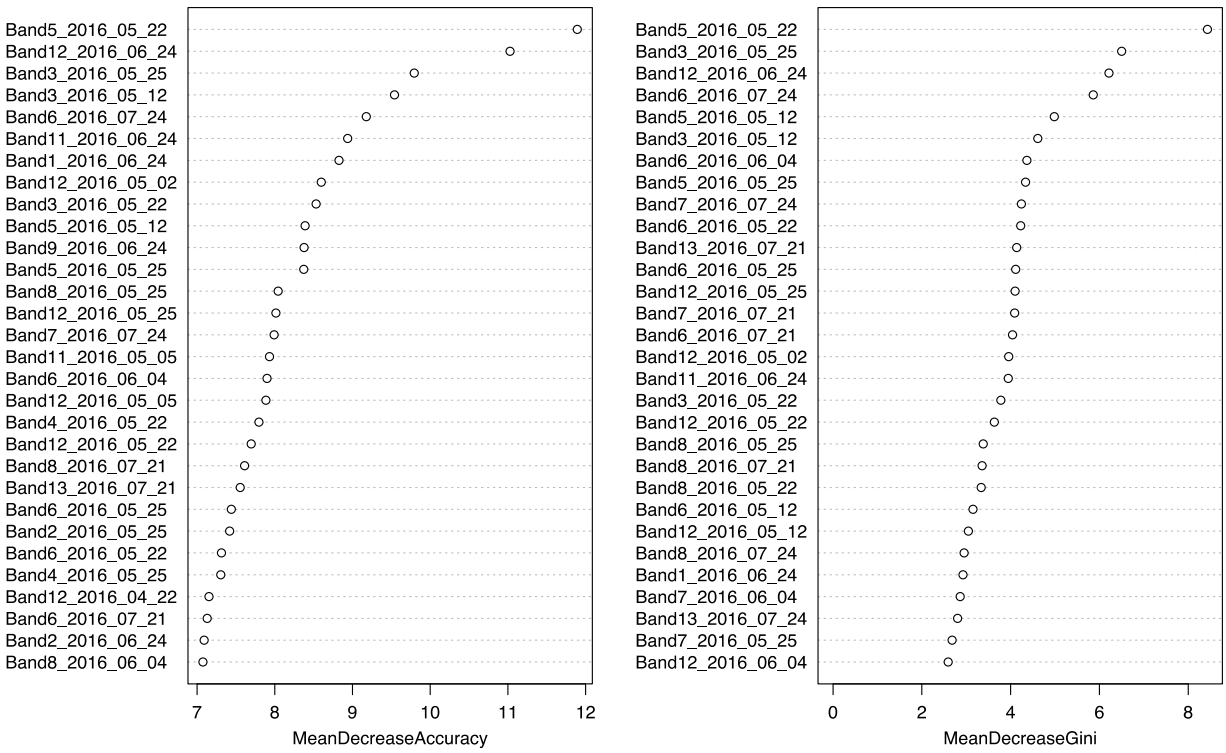

Variable Importance RF S2–VI pixel based

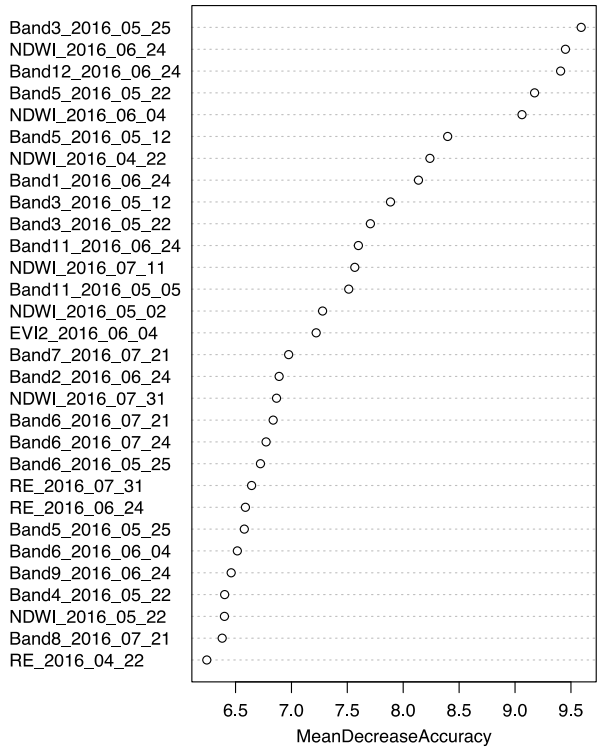

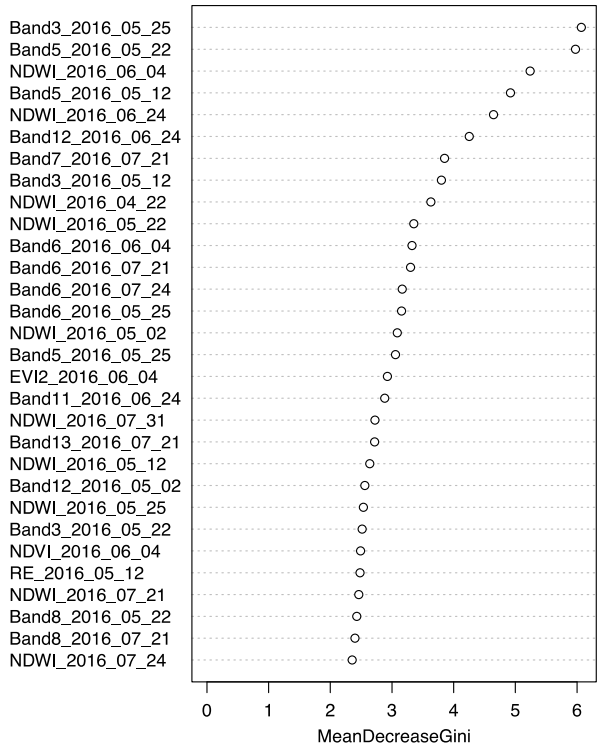

Variable Importance RF S1–S2–VI pixel based

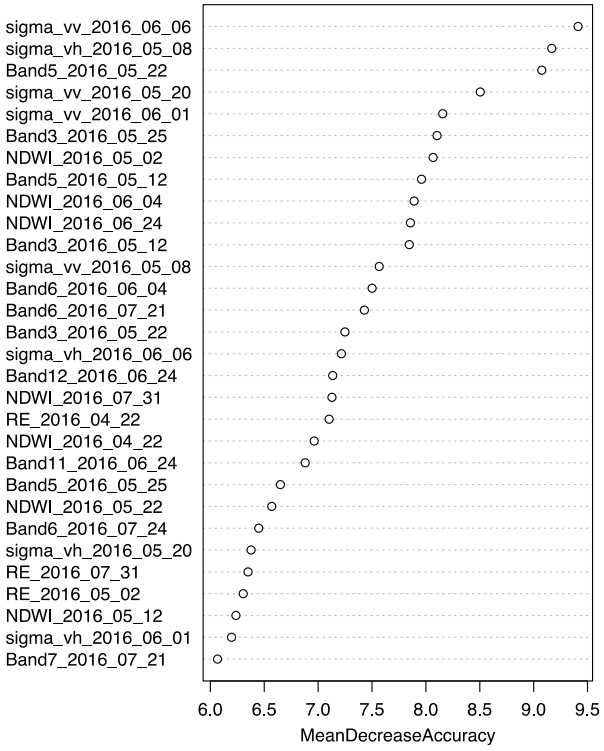

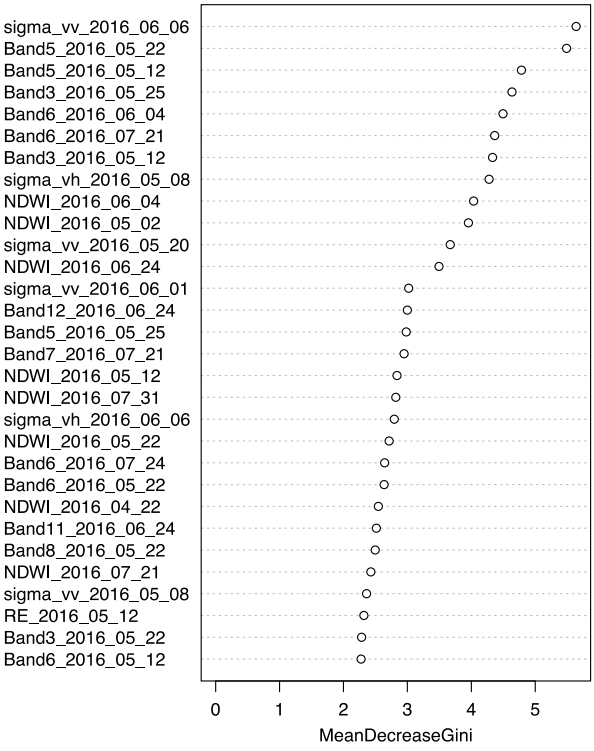

Variable Importance RF S1 object based

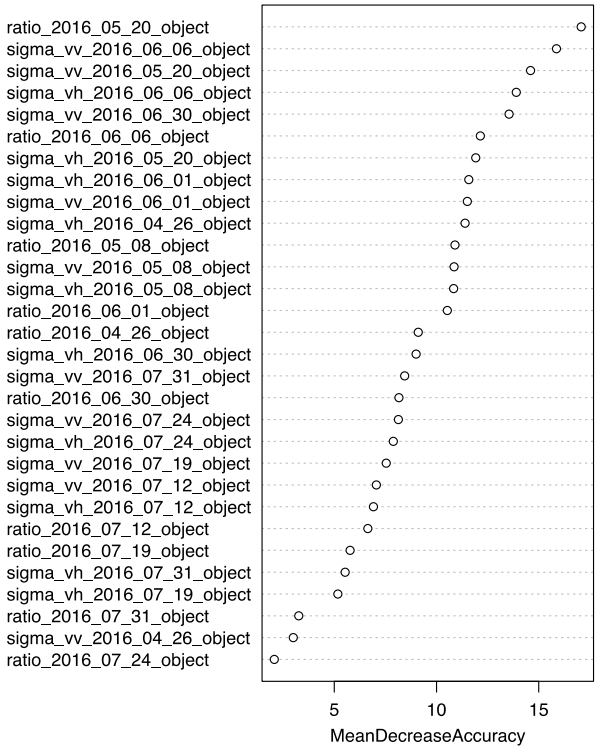

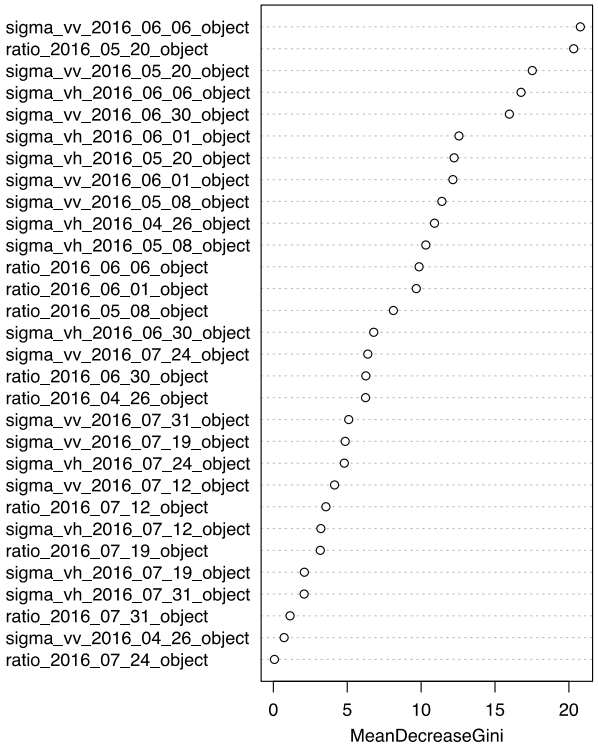

Variable Importance RF S2 object based

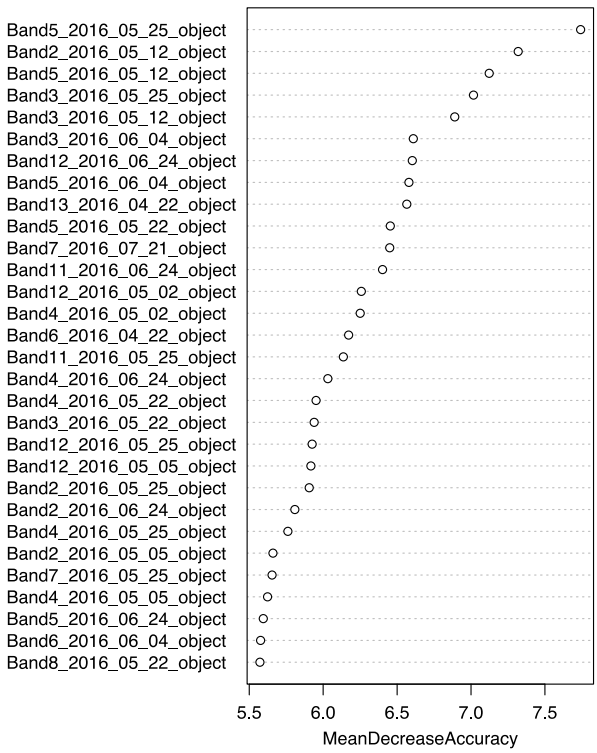

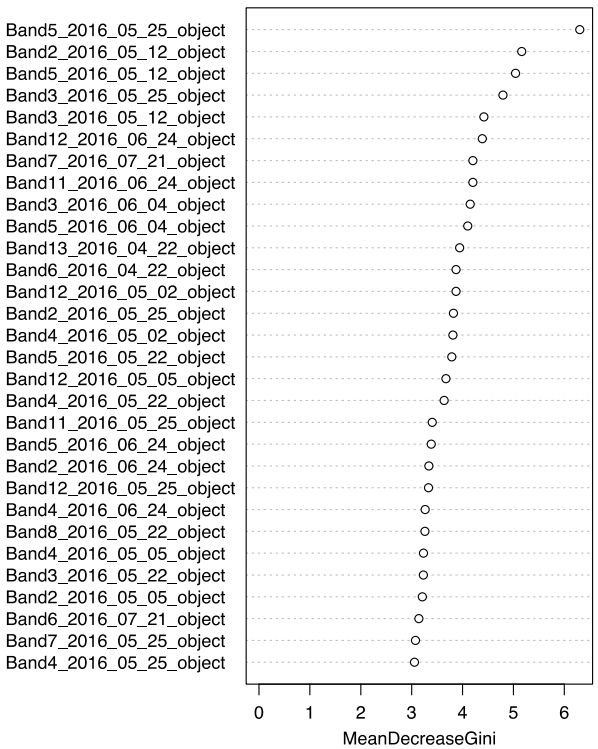

Variable Importance RF S2–VI object based

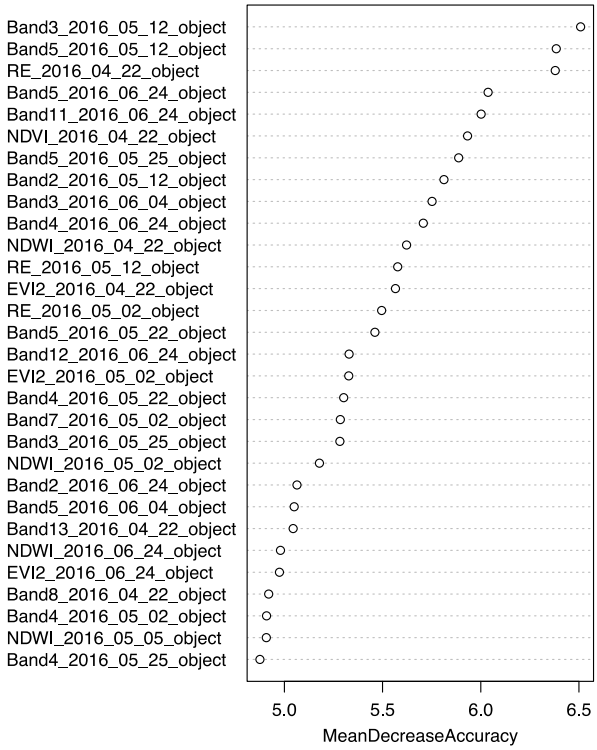

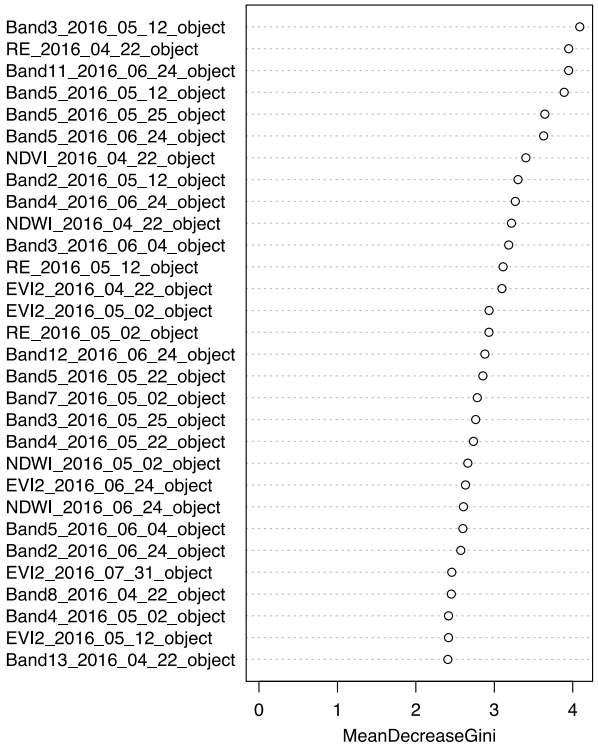

Variable Importance RF S1–S2–VI object based

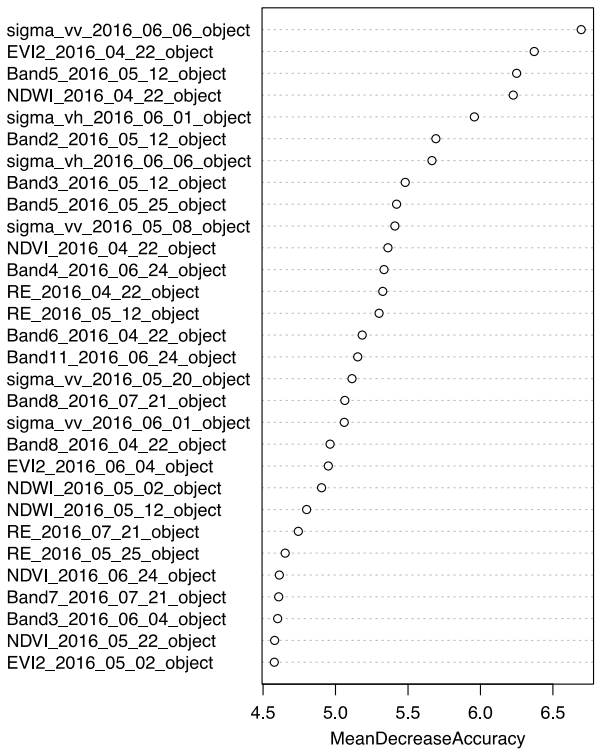

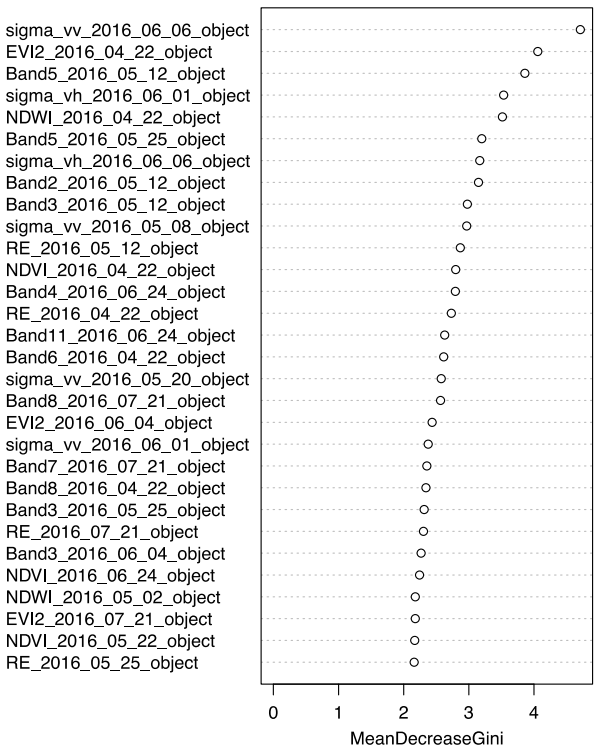

Department of Physical Geography and Ecosystem Science, Lund University

Lund University GEM thesis series are master theses written by students of the international master program on Geo-information Science and Earth Observation for Environmental Modelling and Management (GEM). The program is a cooperation of EU universities in Iceland, the Netherlands, Poland, Sweden and UK, as well a partner university in Australia. In this series only master thesis are included of students that performed their project at Lund University. Other theses of this program are available from the ITC, the Netherlands (www.gem-msc.org or www.itc.nl).

The student thesis reports are available at the Geo-Library, Department of Physical Geography and Ecosystem Science, University of Lund, Sölvegatan 12, S-223 62 Lund, Sweden. Report series started 2013. The complete list and electronic versions are also electronic available at the LUP student papers (https://lup.lub.lu.se/student-papers/search/) and through the Geo-library (www.geobib.lu.se).

1 Soheila Youneszadeh Jalili (2013) The effect of land use on land surface temperature in the Netherlands
2 Oskar Löfgren (2013) Using Worldview-2 satellite imagery to detect indicators of high species diversity in grasslands
3 Yang Zhou (2013) Inter-annual memory effects between Soil Moisture and NDVI in the Sahel
4 Efren Lopez Blanco (2014) Assessing the potential of embedding vegetation dynamics into a fire behaviour model: LPJ-GUESS-FARSITE
5 Anna Movsisyan (2014) Climate change impact on water and temperature conditions of forest soils: A case study related to the Swedish forestry sector
6 Liliana Carolina Castillo Villamor (2015) Technical assessment of GeoSUR and comparison with INSPIRE experience in the context of an environmental vulnerability analysis using GeoSUR data
7 Hossein Maazallahi (2015) Switching to the "Golden Age of Natural Gas" with a Focus on Shale Gas Exploitation: A Possible Bridge to Mitigate Climate Change?
8 Mohan Dev Joshi (2015) Impacts of Climate Change on *Abies spectabilis*: An approach integrating Maxent Model (MAXent) and Dynamic Vegetation Model (LPJ-GUESS)
9 Altaaf Mechiche-Alami (2015) Modelling future wheat yields in Spain with LPJ-GUESS and assessing the impacts of earlier planting dates
10 Koffi Unwana Saturday (2015) Petroleum activities, wetland utilization and livelihood changes in Southern Akwa Ibom State, Nigeria: 2003-2015
11 José Ignacio Díaz González (2016) Multi-objective optimisation algorithms for GIS-based multi-criteria decision analysis: an application for evacuation planning
12 Gunjan Sharma (2016) Land surface phenology as an indicator of performance of conservation policies like Natura2000
13 Chao Yang (2016) A Comparison of Four Methods of Diseases Mapping
14 Xinyi Dai (2016) Dam site selection using an integrated method of AHP and GIS for decision making support in Bortala, Northwest China
15 Jialong Duanmu (2016) A multi-scale based method for estimating coniferous forest aboveground biomass using low density airborne LiDAR data
16 Tanyaradzwa J. N. Muswera (2016) Modelling maize (Zea Mays L.) phenology using seasonal climate forecasts
17 Maria Angela Dissegna (2016) Improvement of the GPP estimations for Sudan using the evaporative fraction as water stress factor
18 Miguel G. Castro Gómez (2017) Joint use of Sentinel-1 and Sentinel-2 for land cover classification: A machine learning approach